

**Remote sensing of the interactions between climate variability and glacier dynamics
for an Alpine temperate glacier, from the scale of the decades to hours**

The case of the Haut Glacier d'Arolla

Chrystelle Gabbud

Under the direction of Prof. Stuart Lane
Expert Prof. Frédéric Herman



Cover picture
The Haut Glacier d’Arolla

Viewed from the true right moraine of the glacier that formed during the Little Ice Age (which became ice free in the 1860s) (05/08/2013)

Foreword

This Memoire is written around two main scientific articles and is divided into four parts. Part I includes the general introduction, the main objectives and the justification of the choices of methods and field study. Two scientific papers follow in Part II and III. The first addresses the decadal scale and uses the archival digital photogrammetry method; the second considers the seasonal to the hourly scale and terrestrial laser scanning technology. Part IV summarises the key results and discusses the limitations and wider perspectives related to this research.

In this context, there is some overlap between Parts I/IV and II/III: this is necessary to ensure the independence and classical structure of the articles. All references are listed together at the end of this work.

Acknowledgements

This work would not have been possible without the invaluable assistance of many people throughout the implementation process. In particular, I would like to thank:

- ◆ Prof. **Stuart Lane**, my thesis advisor, for trusting me, for transmitting his passion for alpine geomorphology and his love for the Haut Glacier d’Arolla, for his widespread availability and for having turned this work into an exciting challenge
- ◆ Prof. **Frédéric Herman**, my expert, for the time spent and for his interest
- ◆ PhD Student **Natan Micheletti**, my ally and source of motivation, for guiding me through each stage, for giving me numerous wise advice and an unfailing support
- ◆ PhD Student Mauro Fischer for his fervent interest in my work, for the glacial explanations and for his encouragement
- ◆ My comrades who accompanied me in the field, in particular Mattia, and with whom I could share richly throughout the realisation of this work including Pauline, Prisca, Gilles and Maxime
- ◆ Marj Tonini and Nancy Pellissier for their attentive reading, Nico Bätz for the photogrammetric learning and Jean-Baptiste Bosson and Christophe Lambiel for their share of opinion
- ◆ My family, my friends, essentially Julien, Michèle, Cindy and all those who believed in me
- ◆ The Fondation Herbette for its financial support and the IDYST institute for providing me ideal working conditions and high-quality software
- ◆ HYDRO Exploitation SA for their trust and for providing data of water flow of the Haut Glacier d’Arolla
- ◆ And all those who lent me a hand, gave me advice or contributed to the completion of this work from near or far, helping me achieving this.

Thank you very much !

Summary

Glacier advance and recession are considered as one of the key indicators of climate change by the Intergovernmental Panel on Climate Change (Houghton *et al.*, 1996). Understanding the relationship between climatic variations and glacial responses is crucial. The main objective of this study is to use remote sensing methods to establish the advance and recession history of an unmonitored Alpine valley glacier, the Haut Glacier d'Arolla, in Switzerland, at three different time scales: decadal, seasonal and daily. At the decadal scale, the purpose is to apply archival digital photogrammetry to this glacier with no established advance/retreat history and to use the data generated to explore the linkages between glacier recession and climate forcing. The key question is whether or not archival photogrammetric methods can be used to reconstruct glacial history. At the seasonal and daily scales, the purpose is to show how repeat measurement of a glacier surface using the new generation of laser scanners can be used to study glacier surface ablation and other elements of glacial hydrodynamics. The key question is over what timescale can meaningful results be obtained using an ultra long range LiDAR RIEGL VZ-6000 scanner specifically designed for measurement of snow and ice cover surfaces.

Results from the use of Digital Elevation Models (DEMs) to perform surface and volume changes with high precision show continual recession of the glacier since 1967, associated with long-term climatic amelioration but only a weak response to shorter-term climatic deterioration within this trend. Glacier surface velocity estimates obtained using surface particle tracking showed that, unlike for most Swiss glaciers, ice mass flux from the accumulation zone was too low to compensate for the effects of glacier thinning and subsequent snout recession. At the seasonal and daily scales, the LiDAR was confirmed to be exceptionally powerful as a potential tool for ablation studies. It was shown that spatial variation in seasonal melt was controlled by both aspect and differential debris cover. The daily scale showed the effect of ogive-related debris cover on melt patterns and also revealed possible hydraulic jacking of the glacier snout associated with short term water pressure rises. This latter demonstration brings out how LiDAR may revolutionise cryosphere studies and points to a series of new and important research questions.

Key words

Glacier, Climate change, Digital aerial photogrammetry, Orthoimagery, Terrestrial laser scanning, LiDAR RIEGL VZ-6000, Point cloud, Digital Elevation Model (DEM), surface melt, volumes of melt, Haut Glacier d'Arolla

Résumé

Les avancées et les récessions des glaciers sont considérées comme l'un des indicateurs clés du changement climatique par le Groupe d'Experts Intergouvernemental sur l'Évolution du Climat (Houghton *et al.*, 1996). Comprendre la relation entre les variations climatiques et les réponses glaciaires est crucial. L'objectif principal de cette étude est d'utiliser des méthodes de télédétection pour établir l'avance et la récession historique d'un glacier de vallée alpin sans surveillance, le Haut Glacier d'Arolla, en Suisse, à trois échelles de temps différentes: décennale, saisonnière et journalière. À l'échelle décennale, le but est d'appliquer la photogrammétrie aérienne d'archive sur ce glacier dont l'histoire des avancées/retraits n'a pas été établie et d'utiliser les données générées pour explorer les liens entre la récession glaciaire et le forçage climatique. La question clé est ici de savoir si les méthodes de photogrammétrie d'archive peuvent être ou non utilisées pour reconstruire l'histoire glaciaire. Aux échelles saisonnières et journalières, le but est de montrer comment la mesure répétée d'une surface glaciaire via l'utilisation de la nouvelle génération de scanners laser peut s'avérer utile pour étudier l'ablation de surface des glaciers ainsi que d'autres éléments de l'hydrodynamique glaciaire. La question clé est ici de déterminer sur quelle échelle de temps des résultats significatifs peuvent être obtenus en utilisant un scanner LiDAR RIEGL VZ-6000 à ultra longue portée spécialement conçu pour la mesure des surfaces de neige et de glace.

Les résultats de l'utilisation de modèles numériques de terrain (MNTs) représentant les changements de surface et de volumes avec une grande précision démontrent une récession continue du glacier depuis 1967, associée à l'amélioration du climat à long terme, avec uniquement une faible réponse à la détérioration du climat à court terme par rapport à cette tendance. Les estimations de la vitesse de surface du glacier obtenues par suivi de particules de surface ont montré que, contrairement à la plupart des glaciers suisses, le flux de la masse de glace depuis la zone d'accumulation était trop faible pour compenser les effets de l'amincissement du glacier et de la conséquente récession du front. Aux échelles saisonnières et journalières, le LiDAR a été confirmé comme extrêmement puissant en tant qu'outil potentiel pour les études d'ablation. Il a été démontré que la variation spatiale de la fonte saisonnière était contrôlée à la fois par la radiation solaire et la couverture de débris différentielle. L'échelle journalière a fait ressortir l'effet des ogives en relation avec la couverture de débris sur les modèles de fusion et a également révélé un potentiel soulèvement hydraulique du front glaciaire associé à l'augmentation de la pression de l'eau à court terme. Cette démonstration met en évidence comment le LiDAR peut révolutionner les études de la cryosphère et ouvrir la porte à toute une série de nouvelles et importantes questions de recherche.

Mots-clés

Glacier, Changements climatiques, Photogrammétrie aérienne d'archive, Orthoimagerie, Scannage laser terrestre, LiDAR RIEGL VZ-6000, Nuage de points, Modèle Numérique de Terrain (MNT), fonte de surface, volumes de fonte, Haut Glacier d'Arolla

Part I - Introduction

1.1	Introduction	13
1.2	General methodological justification	14
1.3	Study site choice and justification	14

Part II - 1st article

Response of an Alpine valley glacier to climate change at the decadal scale

2.1	Introduction	19
2.1.1	Climate Change and glaciers in a Swiss context.....	20
2.2	Methodology	21
2.2.1	Study site	21
2.2.2	Reconstruction of x, y, z point clouds and orthoimage production	21
2.2.3	Data processing	23
2.2.4	Management of error and determination of data uncertainty.....	23
2.2.5	Correction of volumes of change for ice mass flux	24
2.2.6	Contextual data	25
2.3	Results	25
2.3.1	Data quality	25
2.3.2	Glacier stages from 1967.....	25
2.3.3	Changes in glacier surface elevation	27
2.3.4	Volumes of surface change	29
2.3.5	Changes in the upstream boundary cross-section	29
2.3.6	Section averaged velocity close to the upstream boundary of volume calculation	30
2.3.7	Volumes of ice mass loss	31
2.3.8	Comparison with water yield from the basin.....	31
2.4	Discussion	33
2.4.1	Data quality	33
2.4.2	Glacier recession and climate forcing	33
2.4.3	Spatial variation in ice melt	35
2.4.4	Linkages between climate forcing and water yield	36
2.5	Conclusions	37
2.6	Acknowledgements	37

Part III - 2nd article

LiDAR measurement of surface melt for a temperate Alpine glacier, at the seasonal and hourly scales

3.1	Introduction	41
3.2	Study area	41
3.3	Methodology	43
3.3.1	Terrestrial laser scanners	43
3.3.2	RIEGL VZ-6000	43
3.3.3	Scans undertaken	43
3.3.4	Point cloud processing.....	44
3.3.5	Data quality	45
3.4	Results	46
3.4.1	Data quality	46
3.4.2	Surface changes at the seasonal scale	46
3.4.3	Surface changes at the intra-day scale.....	49
3.5	Discussion	50
3.5.1	Methodological issues and data quality.....	50
3.5.2	Seasonal surface changes.....	51
3.5.3	Intra-day surface changes	51
3.6	Conclusions	53
3.7	Acknowledgements	53

Part IV - Overall conclusion

4.1	Overall conclusion	57
4.1.1	Glacier recession and climate forcing	57
4.1.2	Glacier melt dynamics at three time scales.....	57
4.1.3	Glacier dynamics at three time scales.....	57
4.1.4	Methodological issues.....	58
4.2	Limits and perspectives	58
4.3	References	61

Part I - Introduction



Chapter picture
The head of the Val d'Hérens

With the Mont-Collon in the centre of the image and the upstream part of the Haut Glacier d'Arolla on the right bank (06/08/2013)

1.1 Introduction

Glacier advance and recession are considered as one of the key indicators of climate change by the Intergovernmental Panel on Climate Change (Houghton *et al.*, 1996). Understanding the relationship between climatic variations and glacial responses is crucial. Various methodologies have been employed to reconstruct past events and to monitor glacier dynamics. In particular, direct and indirect remote sensing technologies offer important opportunities, are developing continually and appear to produce very high quality results if used correctly.

Some of the earliest developments in passive remote sensing followed from the work of Sebastian Finsterwalder who, at the end of the 19th Century, showed that oblique images could be used to reconstruct glacier movement using photogrammetry. Archival digital photogrammetry is particularly powerful when there are historical images available that can be used to reconstruct systems that have not been measured directly. This technique has proved to be particularly valuable in monitoring and reconstructing historical glacier change (e.g. Small *et al.*, 1984; Brecher, 1986; Hubbard *et al.*, 2000; Baltasvias *et al.*, 2001; Kääh, 2001; Keutterling *et al.*, 2006; Barrand *et al.*, 2009; Heid *et al.*, 2012).

One more recent active technique is Terrestrial Laser Scanning (TLS). This method has been used in the geosciences extensively (e.g. Heritage *et al.*, 2007; Alho *et al.*, 2009; Hodge *et al.*, 2009; Smith *et al.*, 2012; Williams *et al.*, 2013) but has a use in cryosphere studies (e.g. Bauer *et al.*, 2003; Avian *et al.*, 2006; Schwalbe *et al.*, 2008) that has been more restricted because the wavelengths typical of terrestrial laser scanners to date are commonly absorbed by snow and ice surfaces except at very short distances. The new generation of laser scanners with ultra long range measurements, although their use is not yet widespread, can solve this problem by using near infrared wavelengths.

The main objective of this memoire is to apply these two remote sensing methods to monitor an Alpine valley glacier, namely the Haut Glacier d'Arolla, in Switzerland, at two different time scales, decadal scale and seasonal scale, to improve the understanding of its dynamics under climate forcing. The primary approach is the reconstruction of Digital Elevation Models (DEMs) and the subsequent computation of surface and volume changes.

At the decadal scale, the purpose is to apply archival digital photogrammetry to this glacier, one with no established advance/retreat history and to use the data generated to explore the linkages between glacier recession and climate forcing. Reconstructions of the recent history of glaciers have been performed through and since the Little Ice Age (e.g. Fagan, 2000; Maisch, 2000; Matthews *et al.*, 2005); and also more recently in relation to recent global warming (e.g. Haeberli, 1990; Abermann *et al.*, 2009; Diolaiuti *et al.*, 2012). Here the focus is on the period 1967 to 2009.

At the seasonal scale, the purpose is to show how repeat measurement of a glacier surface using the latest generation of laser scanners can be relevant to study glacier surface ablation and other elements of glacial hydrodynamics, both seasonally and intra-daily. To do this, an ultra long range LiDAR RIEGL VZ-6000 scanner is used which has a laser 3B specifically designed for measurement of snow and ice cover surfaces.

1.2 General methodological justification

The general objective of the Memoire is glacier monitoring at decadal to daily scales. To determine qualitatively and quantitatively the glacier changes over time, three dimensional data have to be obtained and precise elevation values have to be extracted. In turn, the associated point clouds allow Digital Elevation Models (DEMs) to be built and compared (DEMs of difference). Remote sensing techniques are particularly powerful for this purpose as they provide a potentially continuous surface coverage.

Archival digital photogrammetry is a passive remote sensing method that extracts quantitative 3D point data from historical imagery (Lane *et al.*, 2010). The principle is based on the stereo-matching of two overlapping 2D images to create the depth of field or the elevation of the points (Lane *et al.*, 1993) that is the third dimension. This technique allows rapid DEM production, for historical imagery if the necessary ground control can be obtained. It permits analysis for large spatial extents, ensuring measures of the whole glacier or at least a large part of it, although, given the dependence of the methodology upon stereo-matching, snow covered surfaces may not have the texture necessary for data extraction. The Federal Office of Topography (Swisstopo) has provided high quality aerial images since 1967, which allows decadal study. They also obtained imagery primarily in early Autumn when the glacier snow line is likely to be at its highest. Thus, this technique meets perfectly the objective of studying glacier recession at the timescale of decades.

To detect processes at smaller spatial and temporal scales, this technique is possible with the new generation of drone technologies, but these require very extensive post-processing and have not yet been proven for ice surfaces. Thus, the active terrestrial laser scanning (TLS) methodology was chosen as an alternative. The scanners emit near-infrared laser signals and measure the distance between the laser and the object as function of the time lapse between the emission of the pulse and the detection of the backscattered signal (Cracknell *et al.*, 1991) to produce a point cloud in a coordinate system [X,Y,Z]. With particular capability for measurement of ice and snow covered terrain and a precision of better than one centimetre at distances of up to 6 km, the LiDAR RIEGL VZ-6000 is appropriate for the seasonal and intra-day surveys objectives.

1.3 Study site choice and justification

The catchment of the Haut Glacier d'Arolla is located at the head of the Val d'Hérens, Valais, in the Swiss Alps. This glacier is the source of the river Borgne d'Arolla whose water flows are exploited by HYDRO Exploitation SA¹. The climate of the Haut Glacier d'Arolla is temperate, with warm summers, and cold and fairly wet winters, although this general pattern is strongly affected by local relief (Arnold, 2005). This glacier is strongly affected by climate change as it has been in continual recession even during the cooler and snowier periods when adjacent glaciers (e.g. Tsijiore Nouve, Bas Glacier d'Arolla) advanced (e.g. Zryd, 2001; Fischer *et al.*, in press).

This area is an ideal study site as it has been the subject of numerous scientific publications that have, together, changed the understanding of glacier dynamics and subglacial hydrology (e.g. Sharp *et al.*,

¹ See <http://www.hydro-exploitation.ch/> for further information

1993; Harbor *et al.*, 1997; Nienow *et al.*, 1998; Swift *et al.*, 2002; Mair *et al.*, 2003; Willis *et al.*, 2003; Nienow *et al.*, 2005; Fischer *et al.*, 2011) and the relationship between glaciers and climate (e.g. Brock *et al.*, 2000b; Arnold, 2005; Pellicciotti *et al.*, 2005; Brock *et al.*, 2006; Dadic *et al.*, 2010). However, it is surprising that there is no formal recession history established for this glacier and that questions related to climate forcing at the decadal scale have largely been overlooked. There are also no detailed studies of the spatial patterns of ablation at either the seasonal or daily time scales. Otherwise, the glacier has an excellent set of archival imagery.

In logistical terms, the glacier is readily accessible, relatively safe and it is possible to walk around and on the glacier. A large portion of the glacier is also visible from the true right moraine that formed during the Little Ice Age, which gives a good vantage point of the glacier for application of the TLS.

Part II - 1st article

Response of an Alpine valley glacier to climate change at the decadal scale

The case of the Haut Glacier d'Arolla



Chapter picture
Walking on the Haut Glacier d’Arolla

Julien and Arnaud in direct contact with the ice of the glacier tongue (10/08/2013)

2.1 Introduction

Glacier advance and recession are considered as one of the key indicators of climate change by the Intergovernmental Panel on Climate Change (Houghton *et al.*, 1996). Indeed, they are integrators of climate that is, unlike a weather station which measures the temporal variability of individual variable, glaciers combine them together, with changes manifest as variations in length, surface, volume, thickness or flow rate (Francou *et al.*, 2010). Measuring their change can provide very valuable data on how the cryosphere is responding to the integrated effects of a range of changing parameters.

The international monitoring of glaciers started in 1894. The aims were, on one hand, to better understand the mechanisms associated with glacier variations that had been noted during the Little Ice Age, and, on the other hand, to better comprehend the relation of these processes with climate (Haeberli *et al.*, 1989). Since 1896, the International Glacier Commission has published an annual or multi-year report on the state of worldwide glaciers (e.g. Forel *et al.*, 1896; Mercanton, 1961). The first reports were based on qualitative information about the advance and retreat of glaciers globally. Quantitative measurements became dominant from 1967 with early volume change determinations (Kasser, 1967) and thus mass balance calculations. This idea brought into focus the essential link between climate fluctuations and glacier motion. The first glacier inventories followed and in particular the World Glacier Inventories (WGI) from 1976. By the middle of the 1980s, thanks to the birth of the World Glacier Monitoring Service (WGMS), glacier fluctuations had become recognised as a priority variable in climate system monitoring (WMO, 1983).

The availability of quantitative data on glacier response to climate relies upon either direct measurement or indirect monitoring using often image based methods. The latter has included a suite of satellite and airborne platforms capable of monitoring entire ice sheets. For smaller valley-based glaciers, image based methods need higher ground resolutions, of the order of metres rather 10s of metres. Image based methods become particularly powerful when there are historical images available that can be used to reconstruct systems that have not been measured directly. Photogrammetry, a science initially motivated by the aim of using photographs to quantify glacier recession (Finsterwalder, 1890), has proved to be valuable in monitoring and reconstructing historical glacier change (e.g. Small *et al.*, 1984; Brecher, 1986; Hubbard *et al.*, 2000; Baltsavias *et al.*, 2001; Käab, 2001; Keutterling *et al.*, 2006; Barrand *et al.*, 2009; Heid *et al.*, 2012).

The main objective of this paper is to apply archival digital photogrammetry to an Alpine valley glacier with no established advance/retreat history (the Haut Glacier d'Arolla, Switzerland) and to use the data generated to explore the linkages between glacier recession and climate forcing at the scale of decades. Reconstructions of the recent history of glaciers have been performed through and since the Little Ice Age (e.g. Fagan, 2000; Maisch, 2000; Matthews *et al.*, 2005), and also more recently in relation to recent global warming (e.g. Haeberli, 1990; Abermann *et al.*, 2009; Diolaiuti *et al.*, 2012). This study aims to look at glacier recession at the timescale of decades using imagery available from 1967. The specific objectives are: (1) to apply archival photogrammetric methods to generate high resolution and precise Digital Elevation Models (DEMs) of the glacier using available imagery; (2) to use these to create orthoimagery (that is imagery corrected for the effects of relief and image distortion) and hence to identify the spatial patterns in glacier recession; (3) to use the DEMs to determine surface change by DEMs of difference, and the associated limits of detection arising from the associated data quality; (4) to combine these with estimates of glacier flux to allow determination of ice volume changes; and (5) to consider how climate forcing is related to this glacier response. The paper also uses the opportunity

provided by a gauging station operating throughout the study period to quantify how recession in the snout zone has contributed to water yield.

2.1.1 Climate Change and glaciers in a Swiss context

It is well-established that glaciers are subject to climate changes, which may occur in precipitation, temperature, radiation or all three at the same time. The response of the glaciers is to change the amount and the spatial distribution of the mass accumulation and melt by ablation (Hooke, 2005). Global climate is rapidly changing and Switzerland is particularly affected. Since the beginning of the measurements in 1864, which is also generally taken as the end of the Little Ice Age, average temperature has increased by approximately 0.12 °C per decade thus an increase of 1.7 °C over the period 1864-2011 (OFEV *et al.*, 2013). Although this trend has been punctuated by periods of general cooling, annual temperatures showed a clear upward trend and, since the mid-1980s, all annual means have remained above the reference mean (Figure 1) (MétéoSuisse, 2010).

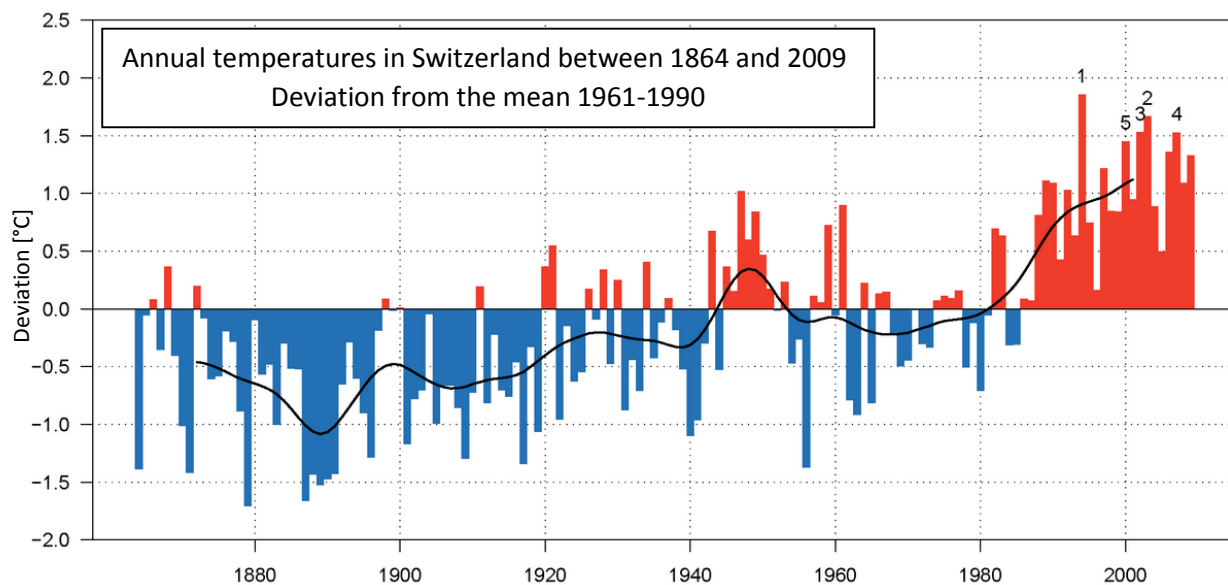


Figure 1: Annual temperatures in Switzerland between 1864 and 2009 in function of the deviation from the reference mean established between 1961 and 1990
In red, years above this mean; in blue, years below this mean; in black, twenty-years weighted average (low-pass Gaussian filter); the numbers indicate hierarchically the hottest years; [MétéoSuisse, 2010]

This figure shows that between the 1960s and the early 1980s, a relatively cooler period occurred after a warmer period in the 1950s. This was followed by a very rapid warming from the mid-1980s which was maintained until present although the increasing trend slowed from the late 1990s onwards. Temperature records since the Little Ice Age are available to the end of the period, and showed 1994 as the hottest year, followed by 2003 and 2002. Unlike temperatures, it is not possible to establish a dominant general trend for the entire Swiss territory regarding precipitation. But for high altitude areas (> 2'500 m), the impacts of climate change on snow cover appear to be negligible (ONERC, 2008). Regarding radiation, sunshine duration decreased significantly until about 1980, before rising again considerably (OFEV *et al.*, 2013).

Globally, similar sorts of changes have been associated with the reduction in the extent of snow and ice masses (IPCC, 2008). Glaciers have been reported to be in a general state of mass balance, but also in a state of retreat (IPCC, 2013). For instance, in Switzerland, almost one third of the total glacierized

area has disappeared since 1973 (Fischer *et al.*, in press). Given the lack of a clear snowfall trend at the altitudes typical of Swiss glaciers, but a clear annual warming trend, it is probable that the recession is an ablation signal, related both to a progressive increase in duration of the melt season and warmer temperatures within that season (Occc *et al.*, 2007). Progressive loss of the ice mass store may cause a catchment to move from a glacial regime, where melt is dominant in the period July through to September, to a nival-glacial regime where there is greater proportionate contribution from snow melt, that occurs in spring as well as summer, and where the reduced glacier stock makes water yield more dependent upon interannual variability in snow fall (Occc *et al.*, 2007).

2.2 Methodology

2.2.1 Study site

The catchment of the Haut Glacier d'Arolla is located at the head of the Val d'Hérens, Valais, in the Swiss Alps. This temperate glacier measures 3.46 km² (Fischer *et al.*, in press). Its accumulation in terms of its firn zone is mainly between the top of the Grande Arête north (3355 m), the Mont Brûlé south (3578 m) and The Vierge to the west (3232 m). The glacier currently flows to an altitude of 2579 m and its mean elevation is 2987 m (Fischer *et al.*, in press). Its average surface slope is relatively flat at 16.9° and its direction is north to north-west in the ablation zone. The glacier lies primarily on a bed of unconsolidated sediments with some bedrock outcrops (Hubbard *et al.*, 1997). This glacier is the source of the river Borgne d'Arolla whose water flows are exploited by HYDRO Exploitation SA². The climate in the area is temperate, with warm summers, and cold, fairly wet winters, although this general pattern is strongly affected by local relief (Arnold, 2005).

This area has been the subject of numerous scientific publications that have, together, changed the understanding of glacier dynamics and subglacial hydrology (e.g. Sharp *et al.*, 1993; Harbor *et al.*, 1997; Nienow *et al.*, 1998; Swift *et al.*, 2002; Mair *et al.*, 2003; Willis *et al.*, 2003; Nienow *et al.*, 2005; Fischer *et al.*, 2011) and the relationship between glaciers and climate (e.g. Brock *et al.*, 2000b; Arnold, 2005; Pellicciotti *et al.*, 2005; Brock *et al.*, 2006; Dadic *et al.*, 2010). However, there has been almost no attempt to reconstruct the history of glacier recession over recent decades and so to start to provide linkages between this understanding and glacier response over longer time periods.

2.2.2 Reconstruction of x, y, z point clouds and orthoimage production

Archival digital photogrammetry was used to construct Digital Elevation Models (DEMs) from historical imagery. Digital photogrammetry is well-established for glacier monitoring (e.g. Pellikka *et al.*, 2010), mass balance determination (e.g. Baltasvias *et al.*, 2001; Hubbard *et al.*, 2000; Huss *et al.*, 2010) and computation of the volumes of ice mass change (e.g. Keutterling *et al.*, 2006; Barrand *et al.*, 2009). The aerial imagery was provided by the Swiss Federal Office of Topography (Swisstopo), with scales varying between 1:9,000 and 1:25,000. The imagery was scanned by Swisstopo to photogrammetric standard at a resolution of 14 µm. All images were obtained during the months of August and September for: 1967, 1977, 1983, 1988, 1997, 2000, 2005 and 2009. In theory, this provides a 42 year record of glacial

² See <http://www.hydro-exploitation.ch/> for further information

history for the catchment. Table 1 shows the theoretical precision of elevations that might be obtained with these images (after Lane *et al.*, 2010) given their scale and the scanning resolution used.

Table 1: Image scale, theoretical precision and the RMSE globally and by co-ordinate of the bundle adjustment
Also shown is the elevation uncertainty calculated from independent assessment and its propagation into uncertainty of elevation changes and calculated volume estimates (see below)

Year	Image scale, x (1: x)	Theoretical precision (m)	Global RMSE of bundle adjustment (m)	RMSE X (m)	RMSE Y (m)	RMSE Z (m)	Mean error Z (m)	σ_i (m)	$dz_{i-1,i}$ (m)	$\sigma_{v, i-1, i}$ (m ³)
1967	13'700	±0.19	±0.59	±0.83	±0.81	±0.04	0.00	±0.04		
1977	10'000	±0.14	±0.39	±0.21	±0.23	±0.01	0.00	±0.01	±0.082	±4'886
1983	12'000	±0.17	±0.35	±0.18	±0.25	±0.08	0.02	±0.09	±0.177	±8'582
1988	22'200	±0.31	±0.88	±0.42	±0.62	±0.45	0.05	±0.49	±0.981	±39'645
1997	9'000	±0.13	±0.36	±0.53	±0.45	±0.06	0.01	±0.06	±0.973	±29'266
2000	9'000	±0.13	±0.37	±0.39	±0.34	±0.07	0.01	±0.07	±0.190	±3'936
2005	11'900	±0.17	±0.36	±0.33	±0.40	±0.04	0.01	±0.05	±0.172	±2'805
2009	13'000	±0.18	±0.30	±0.34	±0.24	±0.07	0.02	±0.07	±0.163	±1'956

Application of digital photogrammetry required ground control points (GCPs) to be visible on the images used for DEM determination. However, as this study uses historical imagery obtained for other purposes, GCPs were not available. Thus, archival digital photogrammetric methods were applied (e.g. Chandler, 1999; Lane *et al.*, 2010). These use points that can be confidently identified as stable over the timescale of the study, in a two steps process: (1) the positions of such points are obtained with differential GPS (dGPS); and (2) these are mapped onto 50 cm orthoimagery, provided by Swisstopo for 2004, to check that they are located within generally stable zones. The dGPS data were obtained by Leica SR530 and Trimble R10 GNSS/GPS/Glonass systems using the Real-Time Kinematic (RTK) method. Measurements were made with reference to a fixed and continually logging base station. The co-ordinates of the latter were post-processed using the Swiss AGNES network of continually recording dGPS stations and transformed into the Swiss coordinate system CH1903+. All GCPs measured for the photogrammetry were then post-processed to this base station. A total of 51 GCPs were mapped initially and of these about 20 were deemed to be identifiable and stable (lateral displacements of < ±0.3 m, that is commensurate with image resolution). However, these were not uniformly distributed in space, because of constraints associated with access to certain parts of the basin and because much of the basin contained unstable ground (e.g. ice cored moraine).

All the computational operations were performed in the Leica Photogrammetry Suite of ERDAS IMAGINE® 2008. Camera Calibration Certificates provided by Swisstopo were used to remove lens distortion and to establish the interior geometry of the images (the principal points of autocollimation (PPA) and symmetry (PPS), the focal length and the fiducial marks). The exterior orientation (i.e. the positional elements X_0, Y_0, Z_0 and the angular and rotational elements ω (around the X axis), ϕ (around the Y axis) and κ (around the Z axis)) were determined in a simultaneous bundle adjustment using the field measured dGCPs. Automatic generation of tie points was used to improve the precision of the bundle adjustment, with the objective that the root mean square error (RMSE) of the solution (i.e. the fit of the solution) was commensurate with the theoretical precision (as defined by the image scale and the scanning resolution) (Table 1). Tie points are particularly important where the availability of ground control is limited or constrained spatially. By measuring the position of a point on two images, then four measurements (two sets of (x, y) image co-ordinates) are obtained. But this is for a data point with only three unknowns (X, Y and Z), such that there is a net gain of one measurement. Thus tie points can improve the quality of the solution. If the RMSE of the solution is commensurate with

the theoretical precision, then the solution will provide data of a quality that is commensurate with the scale of the imagery.

Once an acceptable bundle adjustment had been obtained for each image date, point data were extracted using stereo-matching, with an average point spacing of 0.30 m. The automated terrain extraction algorithm used was that for mountainous regions (ERDAS, 2009). Initial visual assessment of the point clouds suggested that they were of excellent quality and so it was decided that no further work was required to optimise the stereo-matching algorithm. The point clouds were used to orthorectify the available images to a resolution of 0.3 m.

2.2.3 Data processing

Each point cloud was used to create a Digital Elevation Model (DEM) and a relief shaded model, in the software ArcGIS. The success of the stereo-matching, and the density of point data available (around 16 points/m² on the glacier), meant that a relatively simple nearest neighbour interpolation method gave excellent surface representation. Point clouds were interpolated onto the same XY grid, the latter with a 0.30 m resolution. The orthoimages, aided by the relief shaded model, were manually digitised in ESRI ArcGIS to identify the glacier margin for each date. As snow cover prevented data acquisition on the upper part of the glacier, an upstream boundary common to all dates was chosen, downstream of which data could be reliably used. This meant that the focus of the work was upon recession of the glacier snout.

DEMs of difference were calculated for time-consecutive DEMs and only the glacial. Volumes of ice mass gain/loss were extracted for consecutive time periods from the DEMs of difference, constraining each by the digitised outline for the start of each time period.

2.2.4 Management of error and determination of data uncertainty

During each of the above stages, attempts were made both to minimize error and to quantify any residual data uncertainty. First, in the analysis, the use of dGCPs was restricted to those with a precision within ± 0.050 m after post-processing. The position of the continuously recording base was also corrected to better than ± 0.050 m. Second, as noted above, bundle adjustment solutions were sought and achieved commensurate in terms of their RMSE with the theoretical precision, under the assumption of negligible mean error in the bundle adjustment (Table 1). This suggests that the method will deliver results that are optimal given the image scale and scanning resolution.

Third, in the analysis, more GCPs than the minimum necessary were always added to calculate a solution to the bundle adjustment. This allowed to compare the fitted GCP positions to their field measurements and so to calculate a mean error and a standard deviation of error (σ_i) (Table 1) for each date i . This standard deviation was applied to the sum of the control points residual values. In all cases, the mean error was found to be negligible (< 0.05 m) (Table 1). That is, there was no major systematic bias in the solutions. However, this overlooks the fact that the precision of individual data points will not be zero and if the mean error is negligible, it is the point precision that controls the magnitude of change necessary to be deemed significant (Lane *et al.*, 2003). Thus, for each pair of datasets being compared, under the assumption that the precision is Gaussian, random, and uncorrelated between the pair of datasets being considered, the detectable level of change, with a 95 % confidence, was defined as (Lane *et al.*, 2003):

$$|dz_{i-1,i}| > 1.96 * \sqrt{\sigma_{i-1}^2 + \sigma_i^2} \quad [1]$$

This was used to quantify the magnitudes of change detectable (Table 1) when comparing datasets. It was also used to determine the uncertainty in the volume of change estimates (Table 1) using (Lane *et al.*, 2003):

$$\sigma_v = Ar^2 dz_{i-1,i} \quad [2]$$

with A = the area used for volume of change computation; and r = the resolution, in this case 0.3 m.

2.2.5 Correction of volumes of change for ice mass flux

Volumes of ice mass gain or loss cannot be determined directly from volumes of change without correction for ice mass flux. The 1D mass balance of a glacier can be determined from (Cogley *et al.*, 2011):

$$\frac{dV_{ice}}{dt} = \frac{dV}{dt} + A_u \bar{U} \quad [3]$$

where t = time: V_{ice} = the volume of ice mass loss or gain; V = the volume of surface change detected from the DEMs of difference; A_u = the glacier cross-sectional area across the upstream boundary of the glacier; and \bar{U} = the section averaged velocity obtained by glacier surface velocity measured along the upstream boundary multiplied by 0.9 (Kääb, 2001).

The parameter A_u for each date was determined across the upstream section by extracting the altitude along the section from the DEM for each date and combining this with a DEM of the glacier bed (Sharp *et al.*, 1993) interpolated from single point radio echosounding and provided by Dr. I Willis (Cambridge University). As A_u differs for the start year and the end year, a mean of the results was effectuated between the two years of interest.

To estimate \bar{U} , the orthoimages were first used to identify surface displacements from points common to consecutive image pairs. There was too much image decorrelation with the temporal separation of images in this case to allow automated methods (e.g. Scherler *et al.*, 2008), so a manual approach was adopted. Large blocks on the glacier surface were identified and digitised that were common to pairs of orthoimages. Their mean velocity was then calculated between image pairs using the displacement of their X and Y positions (Table 2).

Table 2 : Mean velocity
Normalized by year and with standard deviation from the global mean 4.61 m/y

Period	Mean velocity (m/y)	σ (m/y)
1967-1977	4.97	±0.58
1977-1983	4.39	±0.17
1983-1988	3.62	±0.37
1988-1997	3.75	±0.28
1997-2000	4.61	±0.32
2000-2005	4.11	±0.03
2005-2009	3.60	±0.39

2.2.6 Contextual data

To aid data interpretation, hourly river discharge data for the Haut Glacier d'Arolla were obtained from HYDRO Exploitation SA from 1962. Figure 2 shows the location and an image of the water intake. Temperature and precipitation data were obtained by altitude dependent extrapolation from the station of Sion, a station about 30 km from the snout of the Haut Glacier d'Arolla and 2000 m lower in elevation, using a monthly calculated lapse rate for the region.

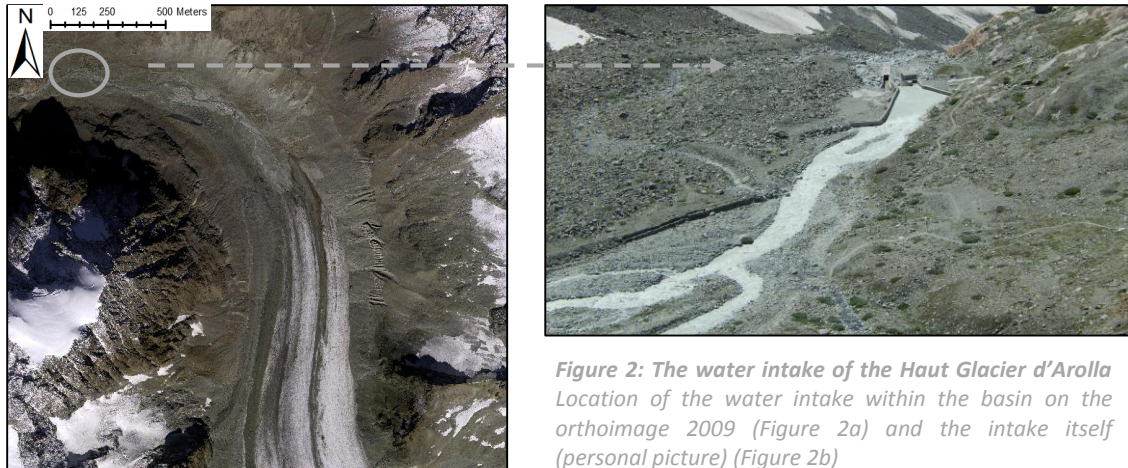


Figure 2: The water intake of the Haut Glacier d'Arolla
 Location of the water intake within the basin on the orthoimage 2009 (Figure 2a) and the intake itself (personal picture) (Figure 2b)

2.3 Results

2.3.1 Data quality

With reference to Table 1, the global RMSE was better than ± 0.90 m in all cases and more precisely better than ± 0.4 m except for the oldest imagery (1967) which had an RMSE of ± 0.59 m, and the imagery with the smallest scale (1988) which had an RMSE of ± 0.88 m. Indeed, there is a general positive association between x in Table 1 and the global RMSE of the solution. As the focus is on vertical changes of ice mass surfaces that were relatively smooth, the Z RMSE is of particular interest. This was better than ± 0.09 m except for 1988. The σ_i indicated that the residuals of the control point standard deviation was similar in magnitude to the RMSE Z reflecting minimal mean error in the solution. Thus, the level of detection possible was always better than ± 1 m. The interpretation of the magnitude of these changes, as well as the volume uncertainty shown in Table 1, depends upon the actual changes measured and this is discussed further below.

2.3.2 Glacier stages from 1967

Figure 3 shows the glacier stages from 1967. The positions of the ice front show a continuous retreat of the glacier snout, with no advance during the cooler periods shown in Figure 1. The glacier snout also narrows both in length and in width. From 1967 to 1988, snout recession was mainly along a West-East line. Notably from 1988 onwards, given the valley morphology, recession was oriented North-North-West to South-South-East and became markedly greater in the middle of the snout than in the partially debris-covered moraines on the glacier margins.

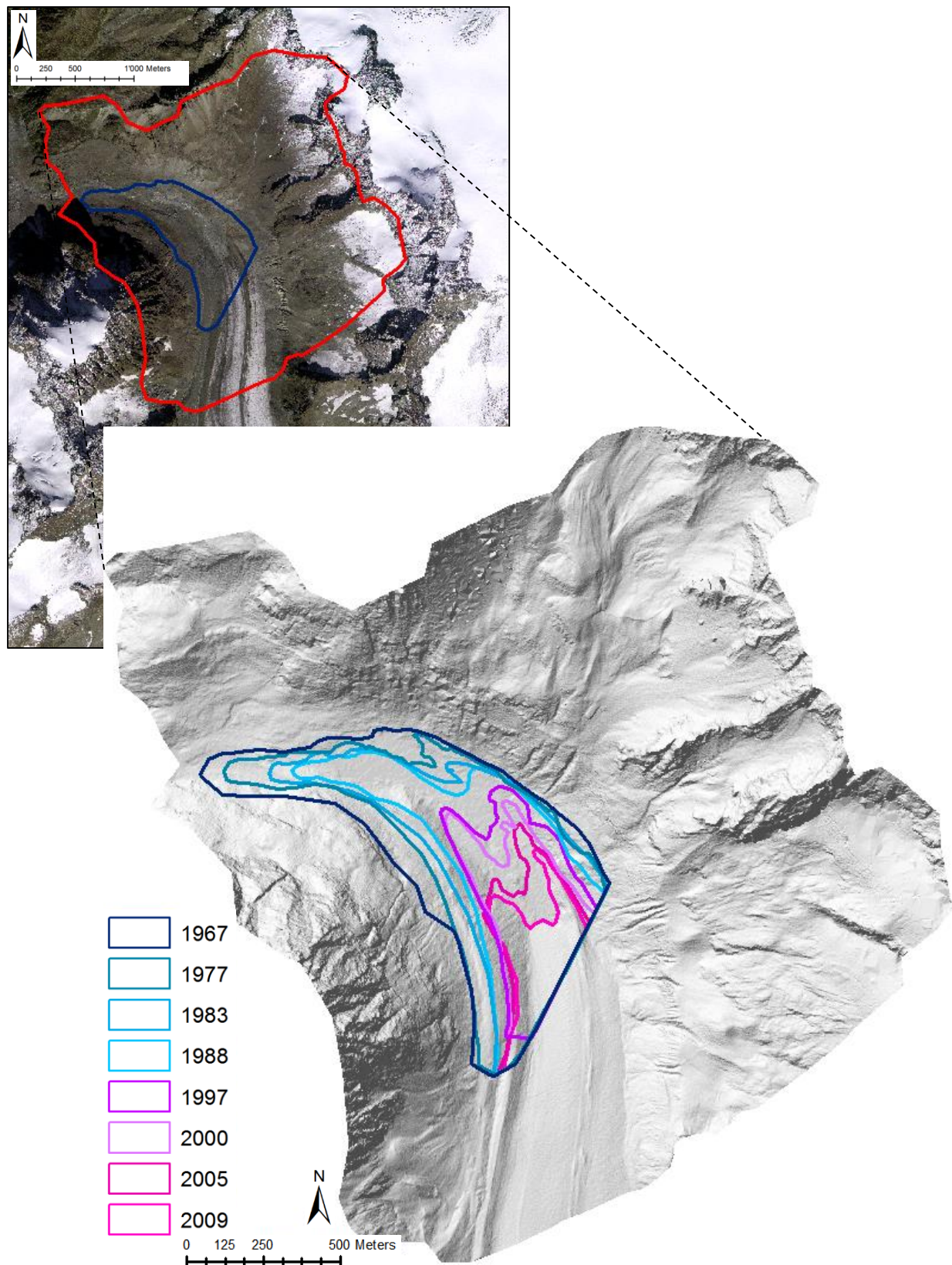


Figure 3: Haut Glacier d'Arolla stages since 1967

3a, Zone of interest on the orthoimage 2009; the red outline represents the 2009 DEM contour without problematic zones (gaps or exaggerated triangulation);

3b, Focus of the stages on the 2009 relief shaded model with the upstream boundary clearly defined

2.3.3 Changes in glacier surface elevation

The DEMs of difference allowed visualisation of the changes in glacier altitude over the time. Figure 4 illustrates two examples: (1) between 1967 and 2009 representing the entire duration of study; and (2) between 2005 and 2009 representing the most recent period. The Limits of Detection (LoD) were calculated from [1] (and presented in Table 1 as $dz_{i-1,i}$). As the positive changes were negligible, they are not displayed.

Globally, changes between 1967 and 2009 show surface reduction. This represents either ice mass thinning but cannot be taken as the ice volume loss without correction for flux effects. The most significant areas of surface reduction are on the glacier and notably close to the position of the snout in 2009, with around 120 m of surface reduction in 42 years. A gradient in surface loss is visible from this point to the snout position in 1967, no doubt reflecting down glacier reduction in ice mass thickness. A gradient also occurs in the up glacier direction from this point. There is an area with slightly slower rates of surface reduction near the centre line of the glacier which corresponds to the main medial moraine of the glacier. Two areas (blue circles on Figure 4a) on the western Little Ice Age moraine underlined consequent reduction, which indicates the presence of dead ice buried inside rocks and sediments. On the opposite moraine, several channels eroded into the Little Ice Age moraine.

The changes between 2005 and 2009 mirror the full period of data. Surface loss was particularly important at the snout reflecting snout retreat, important either side of the mid glacier medial moraine, and lowest on the medial moraine. The downstream region where the ice was trapped by debris (blue circle on Figure 4b) was highlighted as well. Channel erosion was also present on the eastern moraine.

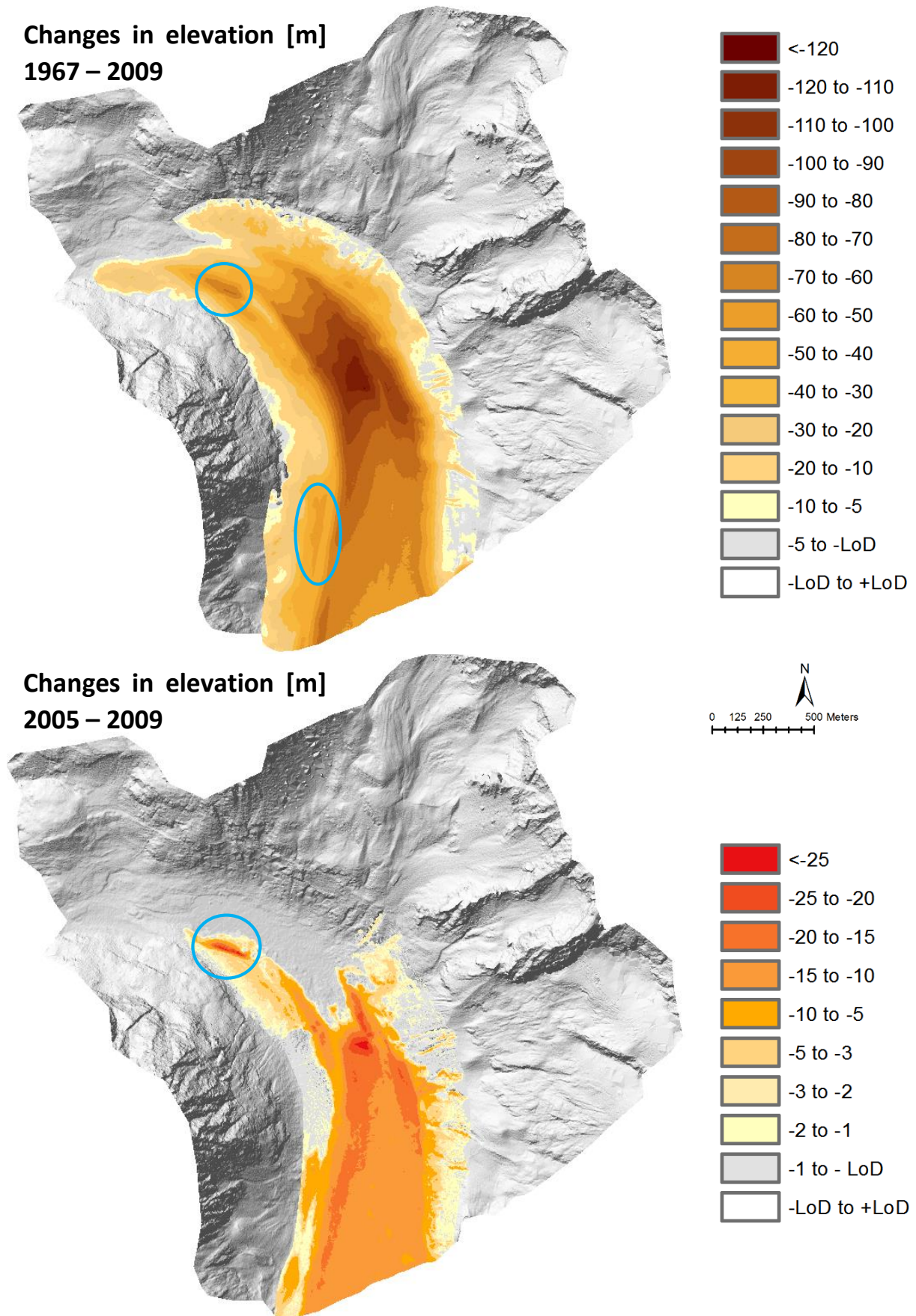


Figure 4: DEMs of difference – erosion; with LoD, on the relief shaded model 2009
4a, The global volumes of change between 1967 and 2009 which is the entire period of study;
4b, The volumes of change between 2005 and 2009 which is the most recent period of study

2.3.4 Volumes of surface change

In all periods, the volumes of surface change were involved a loss, but with relatively low uncertainty, between one and two orders of magnitude smaller than the volume loss (Table 3). When expressed per year, the raw volumes had a peak loss between 1977 and 1983, and then decreased. The maximum loss was reached between 1997 and 2000. The rates then diminished until 2009, which is not surprising as the volume of ice that remains becomes progressively smaller. The period 2005-2009 showed the smallest rate of loss.

Table 3: Volumes of ice mass loss

Volumes of surface loss corrected by the flux and with calculated uncertainty

Period	Volume of surface loss associated with glacier (m ³ /year)	A_u (mean for the period) (m ²)	\bar{U} (m/year)	Flux ($A_u\bar{U}$) (m ³ /year)	Volume of ice mass loss (m ³ /year)
1967-1977	743'591 ±4'886	82'664	4.97 ±1.14	410'838 ±94'236	1'154'429 ±94'363
1977-1983	1'017'378 ±8'582	74'436	4.39 ±0.33	326'772 ±24'564	1'344'150 ±26'020
1983-1988	747'548 ±39'645	69'331	3.62 ±0.73	250'977 ±50'611	998'525 ±64'290
1988-1997	596'346 ±29'266	58'757	3.75 ±0.55	220'340 ±32'317	816'686 ±43'599
1997-2000	1'477'138 ±3'936	42'704	4.61 ±0.63	196'865 ±26'903	1'674'003 ±27'190
2000-2005	691'250 ±2'805	34'128	4.11 ±0.05	140'267 ±1'706	831'517 ±3'283
2005-2009	504'120 ±1'956	26'219	3.60 ±0.77	94'387 ±20'188	598'507 ±20'283

2.3.5 Changes in the upstream boundary cross-section

Figure 5 shows the DEM of the glacier bed (after Sharp *et al.*, 2003) with the glacier stages for the period studied. The 2009 DEM is illustrated also, on the right side. Figure 6 shows the cross-sectional area of the glacier along the upstream boundary. Over the period 1967 to 2009, there is a progressive reduction in the upstream boundary area, and this reflects a loss of both width (Figure 3) and thinning. However, it is not continual, with little loss of area until 1988 (and almost no loss between 1983 and 1988) and more rapid loss from thereon. By 2009, at the upstream cross-section, the glacier had lost about 75 % of its initial thickness. The presence of slower rates of thinning, notably between 1967 and 1983 probably reflects the slightly cooler temperatures during this period.

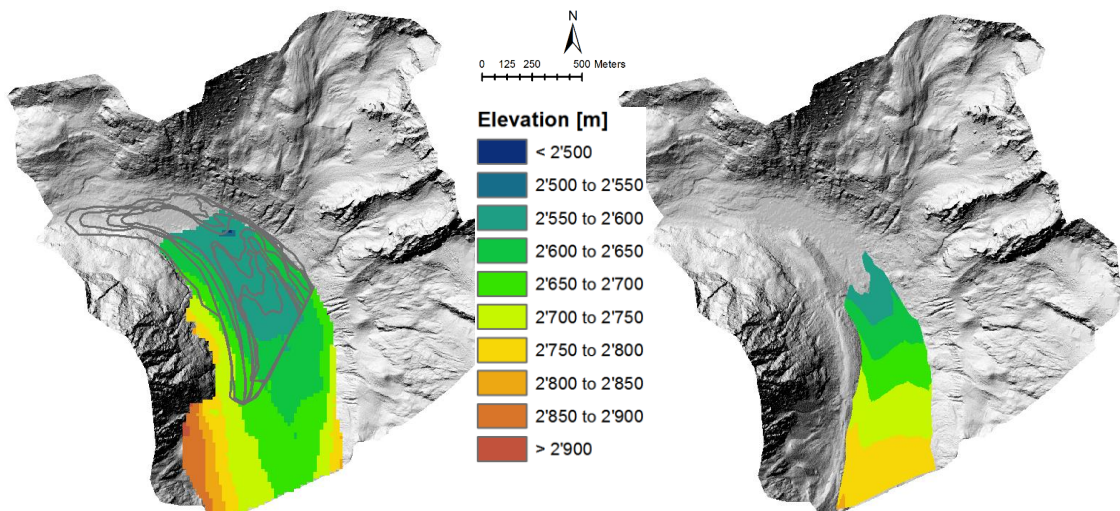


Figure 5: DEM of the glacier bed and DEM of the glacier in 2009

The same colour gradation was conserved; figures are on the 2009 relief shaded model with the boundary cross-section defined by the upstream glacier stages

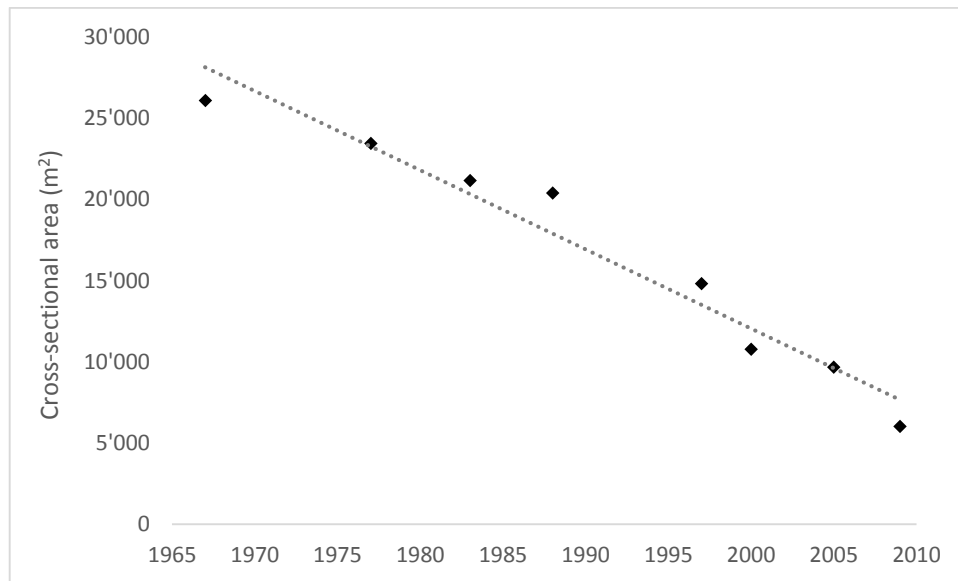


Figure 6: Upstream cross-sectional area

Issued from the thickness along the boundary multiplied by the resolution which is 0.3 m; for each year (not the mean seen on table 3)

2.3.6 Section averaged velocity close to the upstream boundary of volume calculation

Figure 7 shows the section averaged velocity estimated from tracking surface debris blocks. These comprise the combined effects of ice deformation, subglacial sediment deformation and basal sliding (Willis *et al.*, 2003). The flow was more rapid between 1967 and 1977. It decreased progressively until 1988 and quite stagnated until 1997. The period 1997-2000 marked a new increase in the velocity before a gradual deceleration. The uncertainty oscillates between 1 % and 22 % (Table 3).

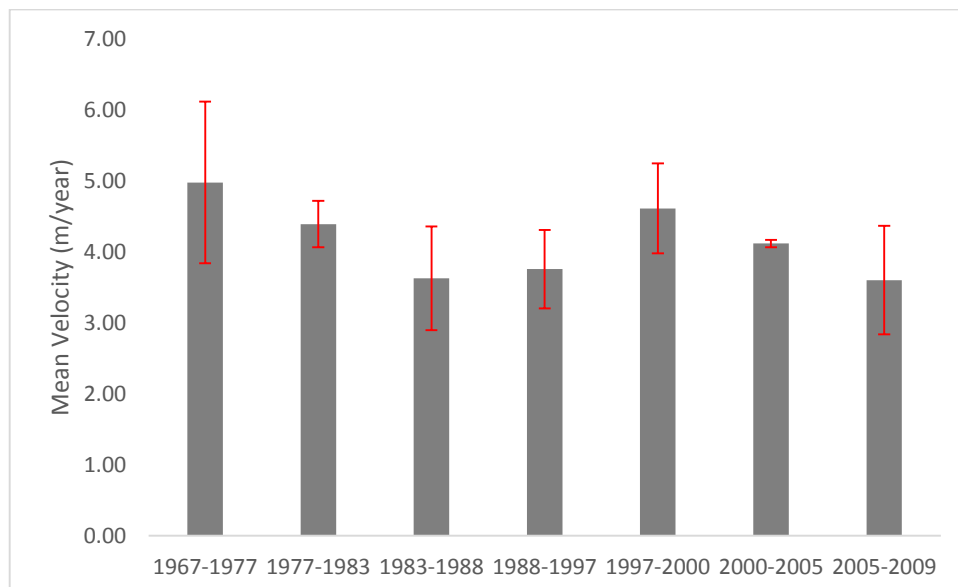


Figure 7: Mean section averaged velocity with the 95 % errors bars as uncertainty

2.3.7 Volumes of ice mass loss

The volumes of surface change, upstream boundary area and velocity data were combined in [3] to calculate the volumes of ice mass loss (Table 3). The annual melting rate, which is the volume of ice mass loss in (m^3/year) divided by the area in (m^2), was also determined (Figure 8). Between 1967 and 1997, the level of melting was relatively constant. The years 1997 to 2000 saw a major increase, with more than $7 \text{ m}^3/\text{m}^2/\text{year}$ of loss. This was lower in 2000-2005 and 2005-2009 but still at a higher level than before 1997.

The flux correction decreases through time, both in absolute terms and also as a proportion of the total ice loss. Glacier thinning, which will reduce the downstream flux, thus contributes to the rapid rate of retreat of the snout.

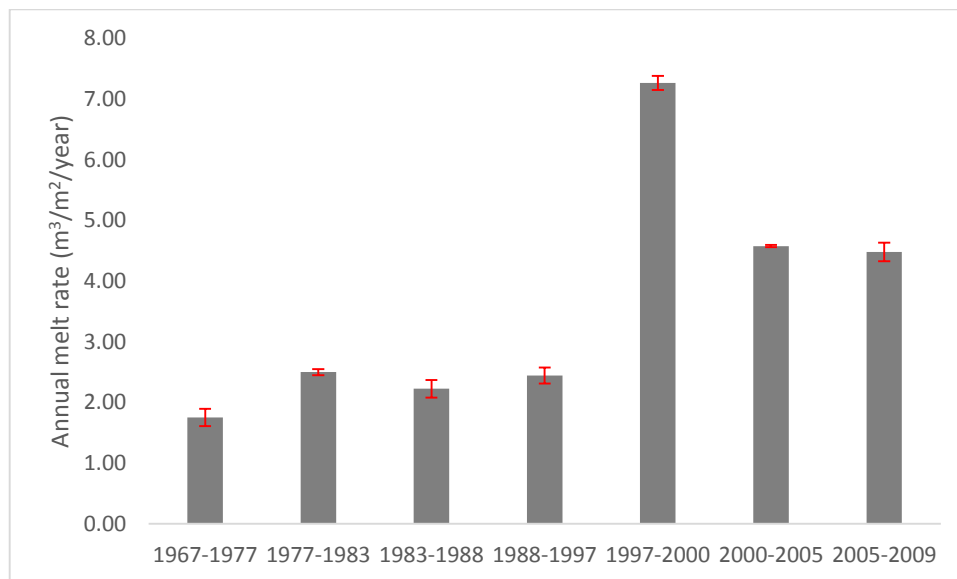


Figure 8: Annual melt rate with uncertainty
The volume of ice mass loss in (m^3/year) divided by the area (m^2)

2.3.8 Comparison with water yield from the basin

The water yield was computed using data from HYDRO Exploitation SA. Figure 9 shows a continual increase in yield, with water production at present about 50 % higher than the 1960s. There was no real trend before 1977 and greater variability until 1997.

This yield comes from annual snowmelt within the catchment as well as glacier ice melt. It is possible to estimate the relative contribution of these variables by normalizing these volumes by year and comparing them to the volumes of ice mass loss (Table 4). The respective density of the water ($1000 \text{ kg}/\text{m}^3$) and of the ice ($917 \text{ kg}/\text{m}^3$) were respected as well. The studied part of the glacier has been responsible for 2 % to almost 6 % of annual flow. However, it was markedly variable, increasing between 1967 and 1983, being lower up until 1997, reaching a maximum contribution between 1997 and 2000, and then declining progressively until its lower level in 2009.

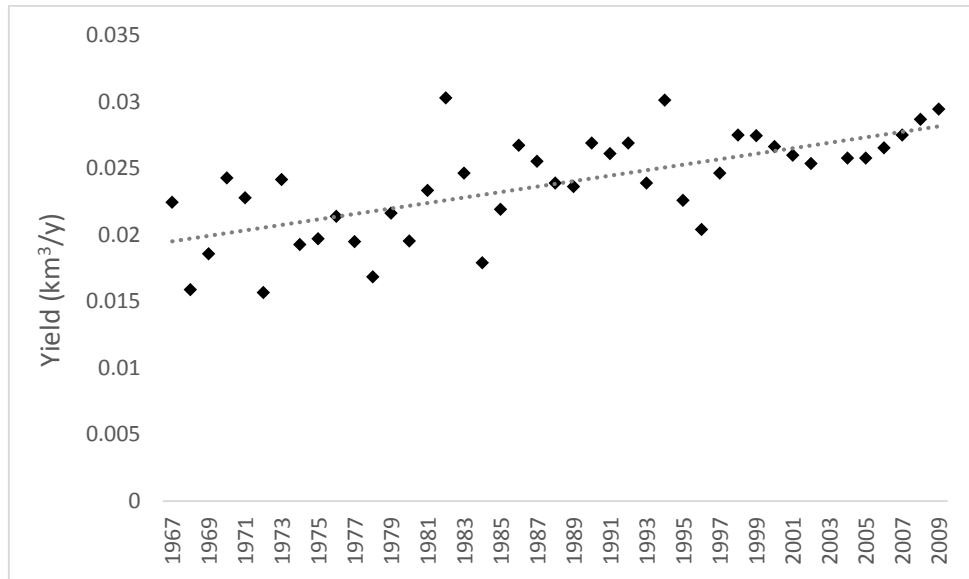


Figure 9: Water yield from the basin between 1967 and 2009

Each year is a civil year; 2003 misses because the data were available only between the months of January and September; the dashed line is the trend line

Table 4: Contribution of glacier ice melt to the water yield

By comparing the measured water volumes at the intake and the volume of ice mass loss

Period	Measured water volume (m³/year)	Volume of ice mass loss (m³/year)	Contribution of study area due to ice melt (%)
1967-1977	20'432'880	1'154'429 ±94'363	5.18 ±0.46
1977-1983	21'870'150	1'344'150 ±26'020	5.64 ±0.12
1983-1988	23'357'340	998'525 ±64'290	3.92 ±0.28
1988-1997	24'951'300	816'686 ±43'599	3.00 ±0.17
1997-2000	26'552'400	1'674'003 ±27'190	5.78 ±0.10
2000-2005	27'057'920	831'517 ±3'283	2.82 ±0.01
2005-2009	27'137'286	598'507 ±20'283	2.02 ±0.07

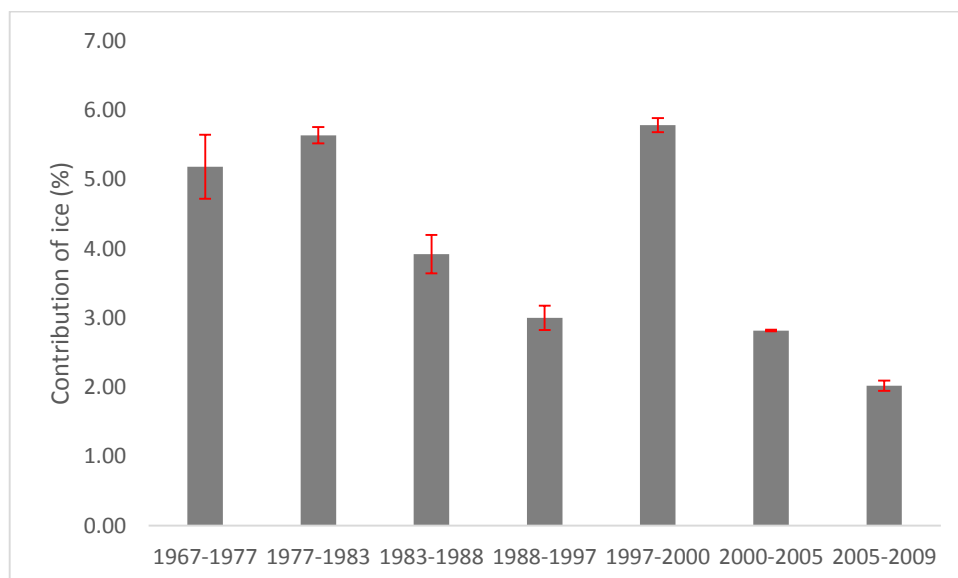


Figure 10: Contribution of glacier ice melt to the water yield, with uncertainty

2.4 Discussion

2.4.1 Data quality

The quality of the results depends firstly on the quality of the imagery available. The aerial images have to be cloud free, shadow free on the zones of interest, without snow cover on the glacier and with a larger scale as possible as scale directly controls the precision of the results obtained. As Table 1 shows, the poorest results were obtained with the smallest scale imagery (note that x in Table 1 is the reciprocal of scale). However, as the data in Table 3 showed, this translates into relatively low uncertainties when multi-year comparisons are being made for a system where the changes at the multi-year scale can be large.

To reconstruct the position and orientation of images, ground control points were required. The quality of the result depended on the quality of the individual data points, the density of data points used and their distribution within the surface (Lane *et al.*, 2003). In this way, the 20 points selected were recorded with better than ± 0.05 m precision to cover as much of the imagery as possible. Nevertheless, some areas were not accessible as the western part and the upper part of the glacier because of unstable and difficult terrain. Thus the South-East part, the sandur and the region of the Refuge des Bouquetins were the best identified. This did not lead to an optimal distribution of control points and meant that tie points were critical in improving the solution.

These issues aside, the error analysis still produced encouraging results: the global RMSE was always better than ± 0.88 m with ± 0.45 m for the Z co-ordinate. The uncertainties in the volumes of ice mass loss after propagation of error were less than 8 % of the measured volume. These low levels of uncertainty suggest that this method can be used to reconstruct snout recession and surface change of otherwise unmeasured glaciers. Moreover, if combined with measurements of surface velocity, it can be used to calculate ice volume changes. Thus, this kind of approach can provide valuable data on glacier response to climate forcing over multiple decades for unmonitored glaciers, where imagery is available.

2.4.2 Glacier recession and climate forcing

As shown in Figure 3, the Haut Glacier d'Arolla has been in continuous recession since 1967, despite the snowier and colder periods recorded in Switzerland in the early 1980s during which most Swiss glaciers advanced (Haeberli *et al.*, 1998). Its continuous recession, without any noticeable advance since the Little Ice Age has been mentioned by others authors (e.g. Alean *et al.*, 2008; Fischer *et al.*, in press).

The annual average melt rate (Figure 8) for the period 1977 to 1983, characteristic of this cooler period, was actually quite similar as the proceeding (1967-1977) and following (1983-1988) periods. The data help to understand why this is the case. In order for the Haut Glacier to advance during the early 1980s, two conditions must be met: (1) the amount of snow and ice accumulation of several years should exceed the amount of ablation (Paterson, 1994); and (2) the accumulation, which will tend to be in the upper part of the basin, must be able to translate to the glacier terminus sufficiently rapidly that it can lead to a glacier advance. Figure 11 and 12 illustrate the temperature and precipitation in Arolla estimated from these of Sion. The annual temperatures were generally lower between 1977 and 1983

when considering the period 1967 to 2009. However, the mean was the same as that of 1967 to 1977. Precipitation increased globally between 1977 and 1983 and was markedly less variable.

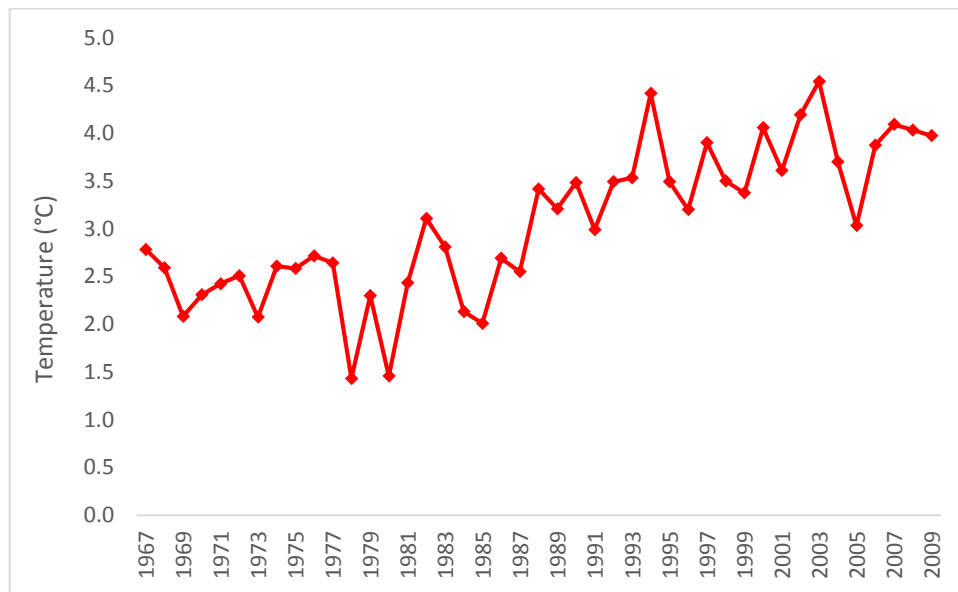


Figure 11: Temperature of Arolla
Estimated from Sion (Lane, 2012)

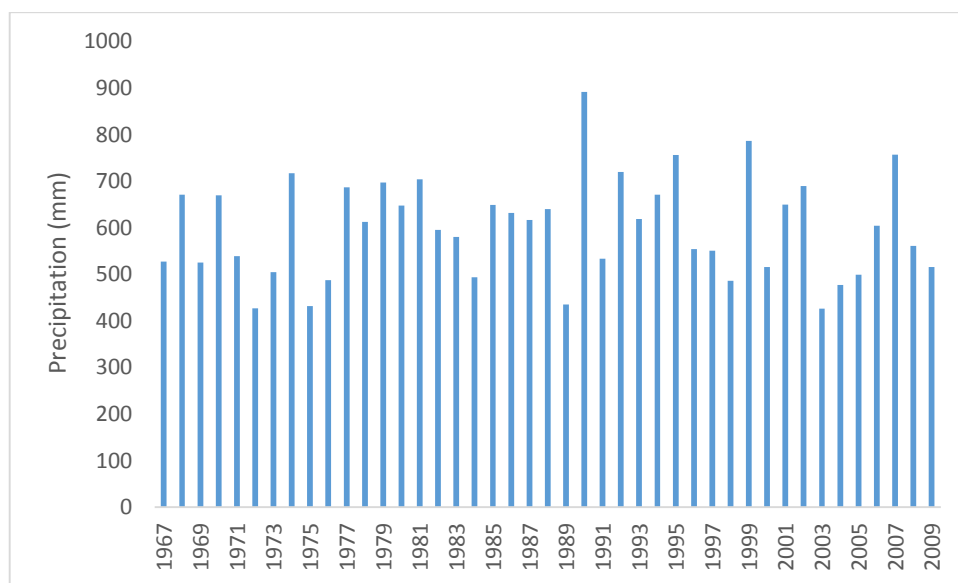


Figure 12: Precipitation of Arolla
Estimated from Sion (Lane, 2012)

It is possible that these conditions combine to create a positive mass balance. Nevertheless, for this to translate into a glacier advance, the upper basin accumulation must translate downstream. The time required for a mass balance perturbation to correct the difference between the steady-state volumes of the glacier before and after the change in mass balance is the response time (Johannesson *et al.*, 1989). If this time is not long enough, the variations are never perceived at the glacier front. This time required will be partly a function of glacier length, the latter positively correlated with the delay between a climatic deterioration and a glacier advance. It will also be a function of glacier velocity. The velocity average of about 4.15 m per year (Figure 7) can be considered as realistic as it matches with others scientific researches on the Haut Glacier d’Arolla (e.g. Harbor *et al.*, 1997: 8 m/year at the center and <2m/year at the glacier margin; Hubbard *et al.*, 1998: mean of 5 to 6 m/year; Mair *et al.*, 2002a;

Mair *et al.*, 2008). Thus if the surface velocities measured for the Haut Glacier d'Arolla (Table 2) are representative of the whole glacier, then the glacier equilibrium line altitude will need to be depressed to very low levels indeed such that accumulation can occur sufficiently close to the glacier snout, and there can be an accumulation-related advance. Thus, the Haut Glacier d'Arolla is less sensitive to short duration increases in accumulation.

The ice flux divergence of a glacier is an important component as it determines the rate of temporal changes of its thickness (Seroussi *et al.*, 2011). For the Haut Glacier d'Arolla, flux was responsible for approximately 35 % of the volume of ice mass loss between 1967 and 1977. This then decreased to about 15 % between 2005 and 2009. As it became less important, it characterised the progressive predominance of ablation, controlled by climate change: the thinning glacier is no longer able to sustain its snout position because of falling flux. As a global warming occurs (Figure 1), it was thus not surprising that the glacier was retreating so rapidly.

The peak in the surface melt rate (Figure 8) between 1997 and 2000 could likewise be the expression of the response time. Although temperature rises from 1986, more slowly from 1992 (Figure 11), it is possible that the response of the system in terms of melt was delayed by an increase in accumulation in the late 1970s and early 1980s: that is, the cooling in this period took time to be perceived at the snout and then, because of the rapid warming, was only capable of slowing the retreat rate, not causing an advance. The dynamics of the glacier was always to melt but not exactly in the same way, always with a lag, which can be in part explained by this response time. More generally, this shows that extreme care must be taken in interpreting data on the recession of glacier snouts in relation to climatic forcing because there will be lags in how a glacier responds to short periods of higher than average accumulation.

2.4.3 Spatial variation in ice melt

The spatial patterns of melt for the entire period and for the period 2005 to 2009 (Figure 4) showed substantial variability, clearly related to the effects of debris cover on melt, and moraine formation. Three medial moraines have been defined for the Haut Glacier d'Arolla: an ablation-dominant moraine east of the glacier centre line, an ice-stream interaction moraine west of the glacier centre line, and a medial-lateral supraglacial moraine complex along the western margin of the glacier (Gomez *et al.*, 1985). Since 1985, the Eastern medial moraine has widened. The western medial moraine and the medial-lateral supraglacial moraine are much less distinguishable because of ice loss between the two. Figure 4b shows how moraine cover can substantially slow ice loss, eventually leading to intact ice-cored moraine: for the period 2005 to 2009, the areas where the melting was more rapid were located on the downstream-centre of the glacier (Figure 4) which were not debris covered (Figure 13). Glacier response to climate fluctuations is strongly influenced by the degree of supraglacial debris cover (Benn *et al.*, 2003). A thin debris cover (<~5 cm) enhances ablation due to a reduced albedo and so an increased absorption of shortwave radiation, whereas thicker debris insulates the underlying ice and reduces ablation, because of its low thermal conductivity (Nakawo *et al.*, 1981). A negative feedback is therefore occurring whereas the moraines develop, and the lateral expanse of moraine cover increases, so parts of glacier become isolated from melt. It leads to downstream extension of medial and lateral moraines beyond the snout terminus (e.g. Figure 13).

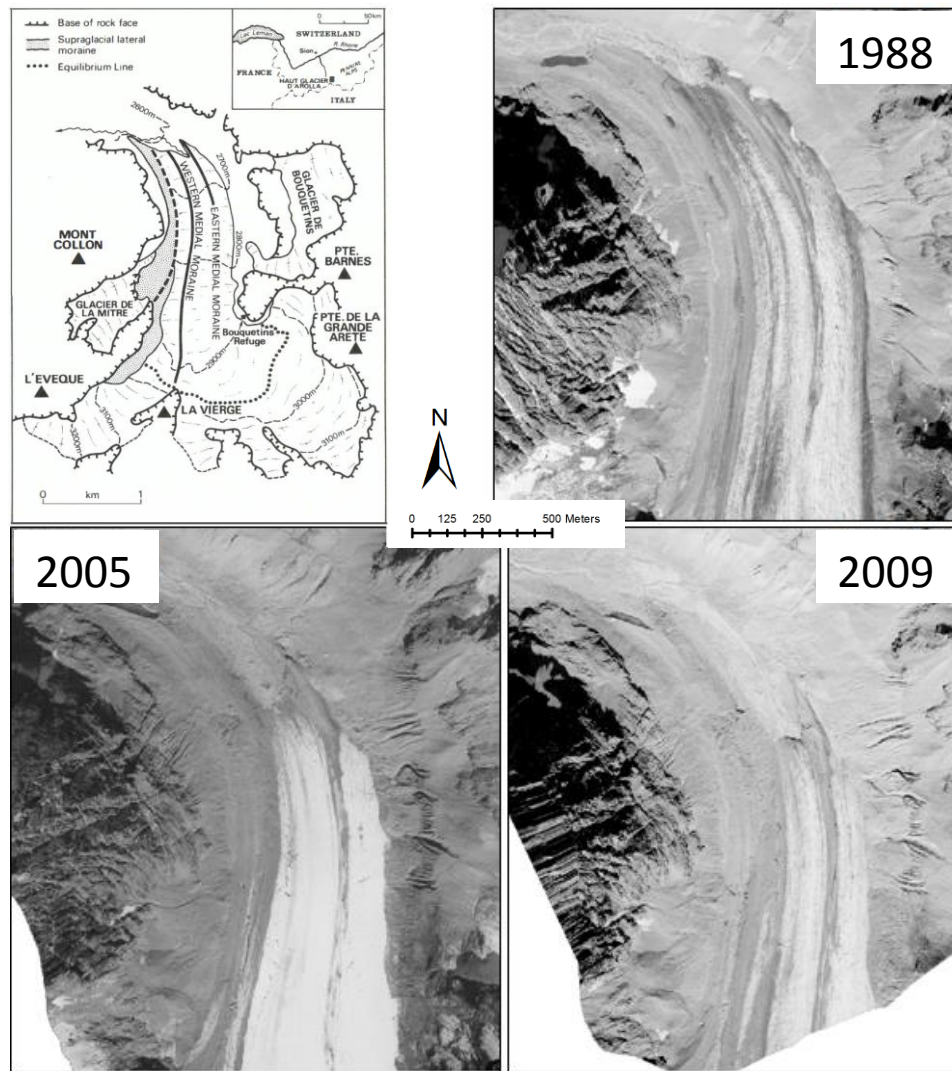


Figure 13: The Haut Glacier d'Arolla three medial moraines
 Map (after Gomez et al., 1985); the evolution of these moraines in 1988 (the closest of 1985 interpretable image), 2005 and 2009 (to illustrate the DEM of difference on Figure 4)

2.4.4 Linkages between climate forcing and water yield

The measured water volumes produced by this catchment increased progressively from 1967 to 2009 (Table 4). The contribution of the ice melt to these volumes did not react except that it has decreased continually as the volume of ice in the studied region falls. However, it does show how the Haut Glacier d'Arolla is losing its net storage of water as ice and that just for the part of the glacier studied, there is a progressive loss of water supply. The volumes calculations do not consider the whole ablation part and the upstream boundaries were the same for all the years (Figure 5). Thus, as the glacier retreats, there was always less ice to melt inside the area considered to the volumes determination.

This assumption is supported by the augmentation of the melt rate (Figure 8) since 2000 as the ice melt contribution to the water yield diminishes. Another explanation could be a diminution of the snow precipitations, which brings less snowmelt but, in the same time, which induce an attenuation of the snow cover protection of the glacier. Thereby, the glacier ice melts faster and the volumes of loss are higher.

2.5 Conclusions

This study demonstrates the potential of archival digital photogrammetry to reconstruct glacier advance and recession. Provided that certain conditions are met, it is possible to generate data with a very good precision in the vertical and so to detect surface changes of better than ± 0.3 m over quite long time periods. Critical to this success is available historical imagery, a glacier surface that is not snow covered, and no cloud cover during image acquisition.

In this study, photography was used from 1967 to 2009 to quantify the dynamics of a glacier that is not in the Swiss Glacier Monitoring database (VAW, 2013). Information generated about the position of the glacier snout demonstrated that the Haut Glacier d'Arolla was in constant recession since 1967. Key explanations as response time were emitted and spatial variation in ice melt was explicated by debris-cover areas. The surfaces changes, the ice mass losses during the period (after correction for flux effects) and their relationship to climate variability were generated as well. In particular, an initial work about the links between the water yield, the glacier behaviour and the climate change was started which have to be pursued, especially from the perspective on the future hydroelectric development exploitation.

2.6 Acknowledgements

This study benefited from financial support from the Fondation Herbette and the University of Lausanne. Special thanks go to the Federal Office of Topography Swisstopo for the provision of aerial images, to HYDRO Exploitation SA for the water flow data, to the Institute of Earth Surface Dynamics (IDYST) of the UNIL for access to the necessary software, and to Mauro Fischer for his comments on earlier parts of the research.

Part III - 2nd article

Lidar measurement of surface melt
for a temperate Alpine glacier, at
the seasonal and hourly scales

The case of the Haut Glacier d'Arolla



Chapter picture
The Haut Glacier d’Arolla with the LiDAR scanner

LiDAR RIEGL VZ-6000 scanner measuring the glacier (30/07/2013)

3.1 Introduction

Methods for detecting changes in glacier volume and their spatial distribution have made increasing use of remote sensing. Some of the earliest developments in remote sensing followed from the work of Sebastian Finsterwalder who, at the end of the 19th Century, showed that oblique images could be used to reconstruct glacier movement using photogrammetry. It is not surprising that, since this early progress, the number of techniques available to measure glaciers using remote sensing has burgeoned, to include (e.g. Iken *et al.*, 1983; Rippin *et al.*, 2003; Mair *et al.*, 2008), radar altimetry and interferometry (e.g. Reinhardt *et al.*, 1986; Andreassen *et al.*, 2002; Herman *et al.*, 2011), digital aerial photogrammetry (e.g. Brecher, 1986; Baltsavias *et al.*, 2001; Keutterling *et al.*, 2006; Barrand *et al.*, 2009; Heid *et al.*, 2012), numerical modelling (e.g. Hubbard *et al.*, 1998; Brock *et al.*, 2000c; Hubbard *et al.*, 2000; Fischer *et al.*, 2011) and airborne laser scanning (e.g. Rees *et al.*, 2007; Notebaert *et al.*, 2009; Deems *et al.*, 2013; Helfricht *et al.*, 2013).

One emerging technique is Terrestrial Laser Scanning (TLS). This has been used in some geosciences extensively (e.g. Heritage *et al.*, 2007; Alho *et al.*, 2009; Hodge *et al.*, 2009; Smith *et al.*, 2012; Williams *et al.*, 2013) but has a use in cryosphere studies (e.g. Bauer *et al.*, 2003; Avian *et al.*, 2006; Schwalbe *et al.*, 2008) that has been more restricted because the wavelengths typical of terrestrial laser scanners to date are commonly absorbed by snow and ice surfaces except at very short distances.

The main objective of this study was to show how repeat measurement of a glacier surface using the new generation of laser scanners can be relevant to study: (1) glacier surface ablation; and (2) other elements of glacial hydrodynamics; over two scales, seasonal and daily. As the time between repetitions shortens, so the magnitude of change should reduce, and so they should become closer to the level of detection determined by instrument related uncertainty. Thus the question is over what timescale can meaningful results be obtained. To do this, an ultra long-range LiDAR RIEGL VZ-6000 scanner was used which has a laser 3B specifically designed for measurement of snow and ice cover surfaces.

3.2 Study area

The catchment of the Haut Glacier d'Arolla is located in the Val d'Hérens, Valais, in the Swiss Alps. The glacier has a surface area of 3.46 km² (Fischer *et al.*, in press), a mean elevation of 2987 m and a snout elevation of 2579 m. Its average slope is 16.9°. The glacier rests on a bed of unconsolidated sediments with some bedrock outcrops (Hubbard *et al.*, 1997). The area has been the subject of extensive scientific research, including subglacial hydrology (e.g. Nienow *et al.*, 1998; Kulesa *et al.*, 2003; Willis *et al.*, 2003), surface ice flow acceleration during spring events (e.g. Mair *et al.*, 2002b; Mair *et al.*, 2003; Mair *et al.*, 2008; Fischer *et al.*, 2011), ice flow velocity (e.g. Harbor *et al.*, 1997), and studies of the controls on surface melt (e.g. Brock *et al.*, 2000a; Hubbard *et al.*, 2000; Pellicciotti *et al.*, 2005; Brock *et al.*, 2006).

The climate of the Haut Glacier d'Arolla is temperate, with warm summers, and cold and fairly wet winters, although this general pattern is strongly affected by local relief (Arnold, 2005). It has been in continual recession since at least the 1960s (Gabbud *et al.*, submitted) even during cooler and snowier

periods when adjacent glaciers (e.g. Tsijiore Nouve, Bas Glacier d'Arolla) advanced (e.g. Zryd, 2001; Fischer *et al.*, in press).

The focus of this study is application of the RIEGL VZ-6000 scanner at the scale of a melt season and at the intra-day scale to measure surface patterns of ice melt in the ablation zone of the Haut Glacier d'Arolla, based upon a scan site located on the true right moraine of the glacier that formed during the Little Ice Age (which became ice free in the 1860s). To do this, two regions were focused upon (Figure 1).

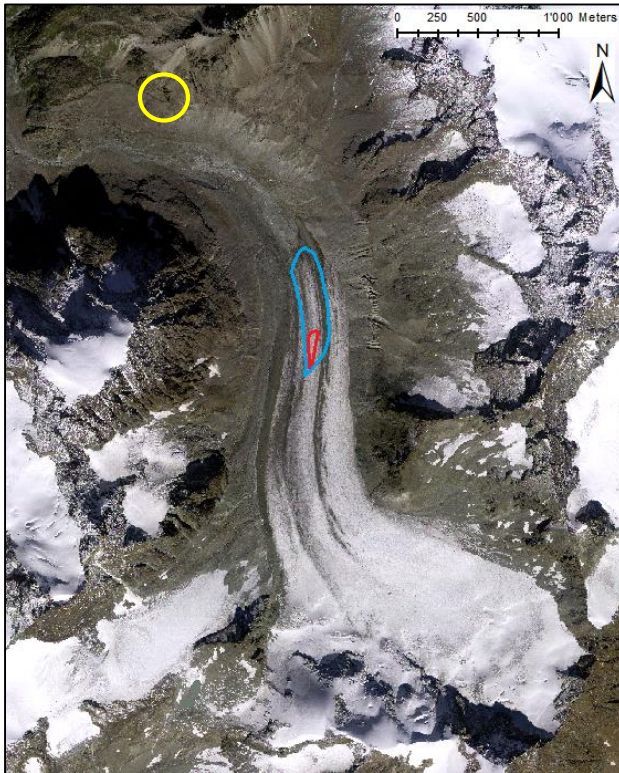


Figure 1: Study site and scans extension

1a, The Haut Glacier d'Arolla on the orthoimage 2009

1b, Picture taken exactly where stood the LiDAR head on the 05/08/2013, representing the field of vision of the scanner

In yellow, LiDAR location; in blue, approximation of the area selected for the seasonal survey; in red, approximation of the area selected for the intra-day survey



3.3 Methodology

3.3.1 Terrestrial laser scanners

Terrestrial laser scanners emit near-infrared laser signals and measure the time required for a return of that signal after reflection from a target of interest. A system of rotation and oscillation of mirrors creates parallel bands of beams which travel in the atmosphere. When they hit a reflector, echos are created. The backscattered signal is captured by a receiver which converts the optical signals into electrical signal. These signals are then digitized and provided to the processor for online waveform processing (RIEGL, 2013c). The distance between the laser and the object is computed as function of the time lapse between the emission of the pulse and the detection of the backscattered signal (Cracknell *et al.*, 1991). This in turn produces a point cloud in a co-ordinate system $[X,Y,Z]$ with the LiDAR head as its origin point $[0,0,0]$ (Figure 2).

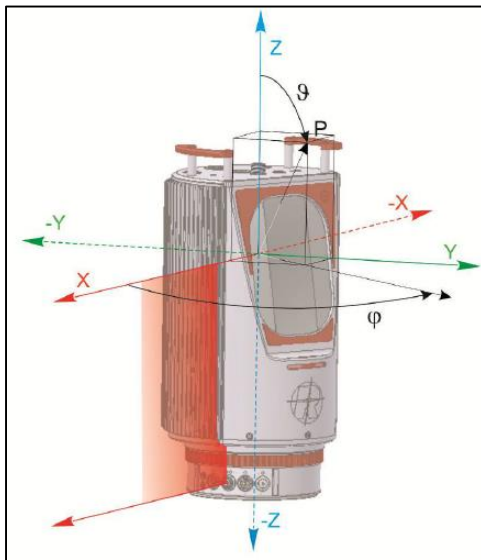


Figure 2: Scanner's own co-ordinate system $[X,Y,Z]$

The rotating polygon mirror deflects the laser beam in a plane P perpendicular to the x/y plane, changing the angle θ ; the rotating optical head rotates in the x/y plane, changing the angle ϕ ; the line scan changes the angle θ , the frame scan changes the angle ϕ (RIEGL, 2013c)

3.3.2 RIEGL VZ-6000

Here, a RIEGL VZ-6000 scanner was used, an instrument that can provide ultra long range measurements (up to 6000 m, according to the reflectivity of the target surfaces) at up to 220'000 measurements per second (RIEGL, 2013a). It has a near infrared wavelength (that is between $0.7 \mu\text{m}$ and 1mm) which means that reflections from snow and/or ice covered terrains are possible even at distances of over 1 km (RIEGL, 2013b). To achieve the latter, the instrument needs to be operated with as low a frequency as possible (here 30 kHz was used). At this frequency, a measurement step of 0.005° is possible, implying an average point spacing of c. 0.09 m at 1 km and c. 0.18 m at 2 km. As the system uses a wavelength classified as a 3B laser, important precautions were taken to protect the eyes of walkers/climbers in the landscape and from reflections back to instrument operators (according to the standards of RIEGL, 2012).

3.3.3 Scans undertaken

A series of scans were performed during the melt season of 2013, using the same measurement position in all cases. The upper part of the glacier was not detectable because of the geometry of the

valley, but the central (about 3 km from the source) and the bottom (about 1 km) portions were clearly visible and were scanned on the following dates: 06/07/2013, 30/07/2013, 05/08/2013, 11/08/2013 and 15/09/2013, at around noon in all cases. To test the capacity of the scanner to measure at a higher frequency, a scan was performed every hour between 9h and 17h on 05/08/2013. For all scans, the decision was taken to use natural features, effectively bedrock outcrops, to orient each scan to the same relative (i.e. local) co-ordinate system during post-processing, the latter established for the 06/07/2013. For this reason, the point clouds covered a larger area than that which was of interest. The Table 1 shows the parameters used in the scans. In particular: (1) the surface area was measured by air view; (2) when the entire scan was acquired in two or three times, the number of points increases because of overlap; (3) the point density is a mean over the surface of interest (the studied portion of the glacier); (4) the intra-day scans were performed each hour, in one shot for 8 minutes.

Table 1: Seasonal (Table 1a) and intra-day (Table 1b) surveys scan parameters

Dates	Surface area scanned (m ²)	Number of points measured	Point density (x/m ²)	Number of scans	Total measurement time (min)
06.07.2013	6'610'785	13'709'776	2.07	2	36
30.07.2013	2'201'591	5'589'410	2.54	2	26
05.08.2013	1'963'256	22'773'067	11.60	3	58
11.08.2013	2'002'014	8'288'364	4.14	2	30
15.09.2013	552'774	7'687'512	13.91	1	12

Time, 05/08/2013	Surface area scanned (m ²)	Number of points measured	Point density (x/m ²)
9h	1'203'484	2'278'934	1.89
10h	1'263'887	2'407'482	1.90
11h	1'432'985	2'735'018	1.91
12h	1'435'513	2'928'132	2.04
13h	1'381'755	2'815'296	2.04
14h	1'463'919	3'304'290	2.26
15h	1'492'458	3'120'042	2.09
16h	1'490'799	2'837'250	1.90
17h	1'594'398	3'302'694	2.07

3.3.4 Point cloud processing

Point cloud processing required a series of steps: (1) joining the overlapped scans to one layer, trimming the data to the area of interest (only the glacier) and removing of clear outliers due for example to atmospheric reflections as dust or moisture, which were minimised through scanning on cloud free days; (2) manually identifying a small number of points to orient and to displace the data approximatively into the same local co-ordinate system; (3) improving the precision of the approximate orientation and overlapping of the scans by comparing automatically only stable points during the period; (4) assessing the quality of each final orientation by minimising the standard deviation while providing sufficient data density to be reliable; (5) transforming the point cloud into a surface (mesh) and manipulating the surfaces to estimate surface change. The software used for processing point clouds from the RIEGL VZ-6000 is RiSCAN PRO® (see RIEGL, 2005 for further details). The processing was undertaken for two separate projects: (1) the seasonal scale; and (2) the intra-day scale; reflecting the fact that the precision of the latter should be better than the former because the instrument was not moved between scans.

For both steps of the registration, the co-ordinate systems for the first seasonal survey (06/07/2013) and the first intra-day survey (09h, 05/08/2013) were used as the datum onto which the others seasonal and intra-day surveys respectively were registered. For the approximate co-registration, a small number (minimum 4) of manually identified common points were used to provide an initial estimate. Then, the density of the point clouds was reduced to facilitate and to shorten the time of computation for the precise orientation, and patches of data associated with bedrock outcrops were identified. Afterwards the precise orientation was undertaken through an iterative closest point process (Zhang, 1992) in which the orientation and the position of each scan were iteratively modified in order to calculate the best fit between the point patches. The output includes an indication of the quality of the fit as a root mean square error.

Each co-registered point cloud was triangulated using nearest neighbour interpolation (a 2D-Delaunay triangulation algorithm) which was judged to be sufficient given the relatively high point density in relation to local variability in surface elevation, but with criteria that limited the maximum length of triangle edges and triangle angles. The maximum edge length was defined as 5 m with the aim of avoiding large data gap while removing too extended triangles. The maximal angle between the triangle normal and the ray of sight was 90° to correspond to the quite flat glacier area.

Finally, the points were exported to the SURFER® software (see Golden Software, 2012 for further details). A regular grid with a 0.3 m spacing (reflecting the approximate point density) was interpolated using kriging. Kriging is a very flexible gridding method based on the regionalized variable theory assuming that the spatial variation in the phenomenon represented by the z-values is statistically homogeneous throughout the surface (Golden Software, 2012) (what was expected for this study). SURFER® uses the variogram model that measures how quickly phenomena changes of the average. A linear component was employed with the slope and the anisotropy equal 1.

The resulting DEMs could be compared by subtraction to visualise surface changes and also to perform volume calculations. It should be noted that the interpolation methods could be improved given that this was a scan from a single point, through consideration of more advanced geostatistical methods.

3.3.5 Data quality

Following Cooper (1998), the derived data could have two types of error: systematic error associated with point errors that are highly inter-correlated (e.g. a clear mean error); and random error associated with individual data points that are locally uncorrelated with one another. Under the assumption that the mean error is negligible and that the random errors are Gaussian and pairwise uncorrelated, the standard deviation of error can be used to identify limits of detection for surface change. To have 95 % confidence in a measured change (Lane *et al.*, 2003):

$$|z_2 - z_1| > 1.96 * \sqrt{\sigma_{z_1}^2 + \sigma_{z_2}^2} \quad [1]$$

where z_i is the elevation of a point at times 1 and 2 and σ_i is the standard deviation of error taken as characteristic of the entire dataset. Thus, this calculation could be used to identify a range for which estimated changes were too small to be statistically significant and so could be considered as noise.

3.4 Results

3.4.1 Data quality

Table 2 shows the standard deviations of error of each compared dataset and the associated limits of detection (LoD) using [1] for each pairwise surface comparison. As the LiDAR was not moved the 05/08/2013 between scans, the standard deviations were significantly smaller (approximately 6 times) as these of the seasonal survey. This is reflected in the LoD also. With these results, it was possible to visualise significant changes in the DEMs of difference.

Table 2: Standard deviation diagonal and Limits of Detection for seasonal scale (Table 2a) and hourly scale (Table 2b)

Dates	06/07/2013	30/07/2013	05/08/2013	11/08/2013	15/09/2013
06/07/2013	±0.000				
30/07/2013	±0.133	±0.068			
05/08/2013	±0.135	±0.189	±0.069		
11/08/2013	±0.114	±0.175	±0.177	±0.058	
15/09/2013	±0.167	±0.213	±0.214	±0.202	±0.085

Time, 05/08/2013	09h	10h	11h	12h	13h	14h	15h	16h	17h
09h	±0.000								
10h	±0.031	±0.016							
11h	±0.031	±0.044	±0.016						
12h	±0.034	±0.046	±0.046	±0.017					
13h	±0.041	±0.051	±0.051	±0.053	±0.021				
14h	±0.035	±0.047	±0.047	±0.049	±0.054	±0.018			
15h	±0.034	±0.046	±0.046	±0.048	±0.053	±0.049	±0.017		
16h	±0.037	±0.048	±0.048	±0.050	±0.055	±0.051	±0.050	±0.019	
17h	±0.039	±0.050	±0.050	±0.052	±0.056	±0.052	±0.051	±0.054	±0.020

3.4.2 Surface changes at the seasonal scale

Table 3 shows the average melt volume per day for each period ($[m^3/day]$) and the same melt volumes divided by the surface to provide an average surface lowering (effectively a melt rate) in $[m^3/m^2/day]$. The same calculations were performed for the intra-day survey in $[m^3/m^2/hour]$. To compare these two time scales, the first melt rate results were normalised by hour also. This calculation assumes that at the scale of the study, there is negligible upstream flux. This assumption is discussed below.

The results are logical and reflect the seasonal evolution of meteorological conditions (Figure 3 - Evolène). The melt rates during July and early August are similar; they then decline gradually during the transition from mid-summer to early autumn. Critical here is the progressive reduction in solar insolation due to the growing effects of valley shading. Averaged over the entire period, for the area studied, the glacier lost approximately $0.05 \pm 0.002 m^3/m^2$ of ice by day during the summer season 2013. Figure 4 illustrated the raw melt rate for each interval of time and the results normalised by day. In practice, the melt rates are thus spatially variable: whilst showing the generally decreasing melt rates through time, there are clear zones of lower melt that trend North-South and which are related to medial moraines (Figure 5). There are some diagonal lines, which are related to small imprecisions in the orientation of individual laser lines. It should be noted that these observations may well underestimate melt because there is no correction for the effects of ice mass flux. Given velocity

measurements made at the Haut Glacier d’Arolla of up to about 1.0 m per year (inferred from Mair *et al.*, 2003), at the timescales being observed, the lateral displacement is not likely to be much more than a single grid cell.

Table 3: Melt volumes and melt rates for the seasonal survey (Table 3a) and the intra-day survey (Table 3b) With the same final melt rate (to help the comparison) and uncertainty

Dates	Number of days	Volume (m ³ /day)	Melt rate (dh) (m ³ /m ² /day)	Melt rate (dh) (m ³ /m ² /hour)
06/07-30/07	24	5'496 ±48	0.059 ±0.001	0.002 ±<0.0001
30/07-05/08	6	5'501 ±273	0.059 ±0.003	0.002 ±<0.0001
05/08-11/08	6	4'022 ±256	0.043 ±0.003	0.002 ±<0.0001
11/08-15/09	35	2'866 ±50	0.031 ±0.001	0.001±<0.0001
06/07-15/09	71	4'011 ±20	0.043 ±0.001	0.002 ±<0.0001

Time, 05/08/2013	Volume (m ³ /hour)	Melt rate (dh) (m ³ /m ² /hour)
9h-10h	13 ±0.45	0.001 ±<0.0001
10h-11h	12 ±0.64	0.001 ±<0.0001
11h-12h	18 ±0.68	0.002 ±<0.0001
12h-13h	12 ±0.78	0.001 ±<0.0001
13h-14h	13 ±0.79	0.001 ±<0.0001
14h-15h	77 ±0.71	0.008 ±<0.0001
15h-16h	18 ±0.73	0.002 ±<0.0001
16h-17h	20 ±0.79	0.002 ±<0.0001
9h-17h	174 ±0.57	0.018 ±<0.0001

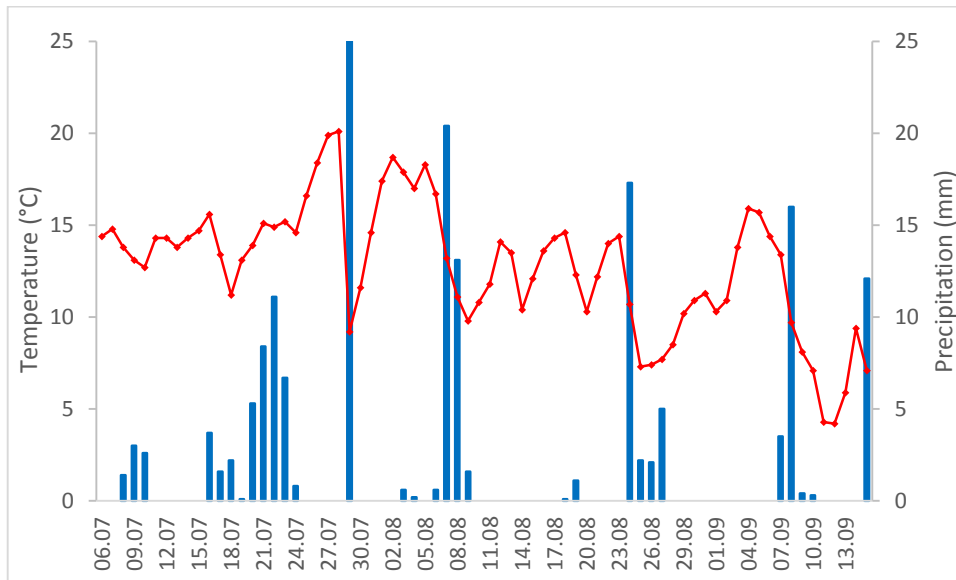


Figure 3: Temperatures and precipitations during the period of study (06/07/2013 to 15/09/2013) These values are issued from Evolène station

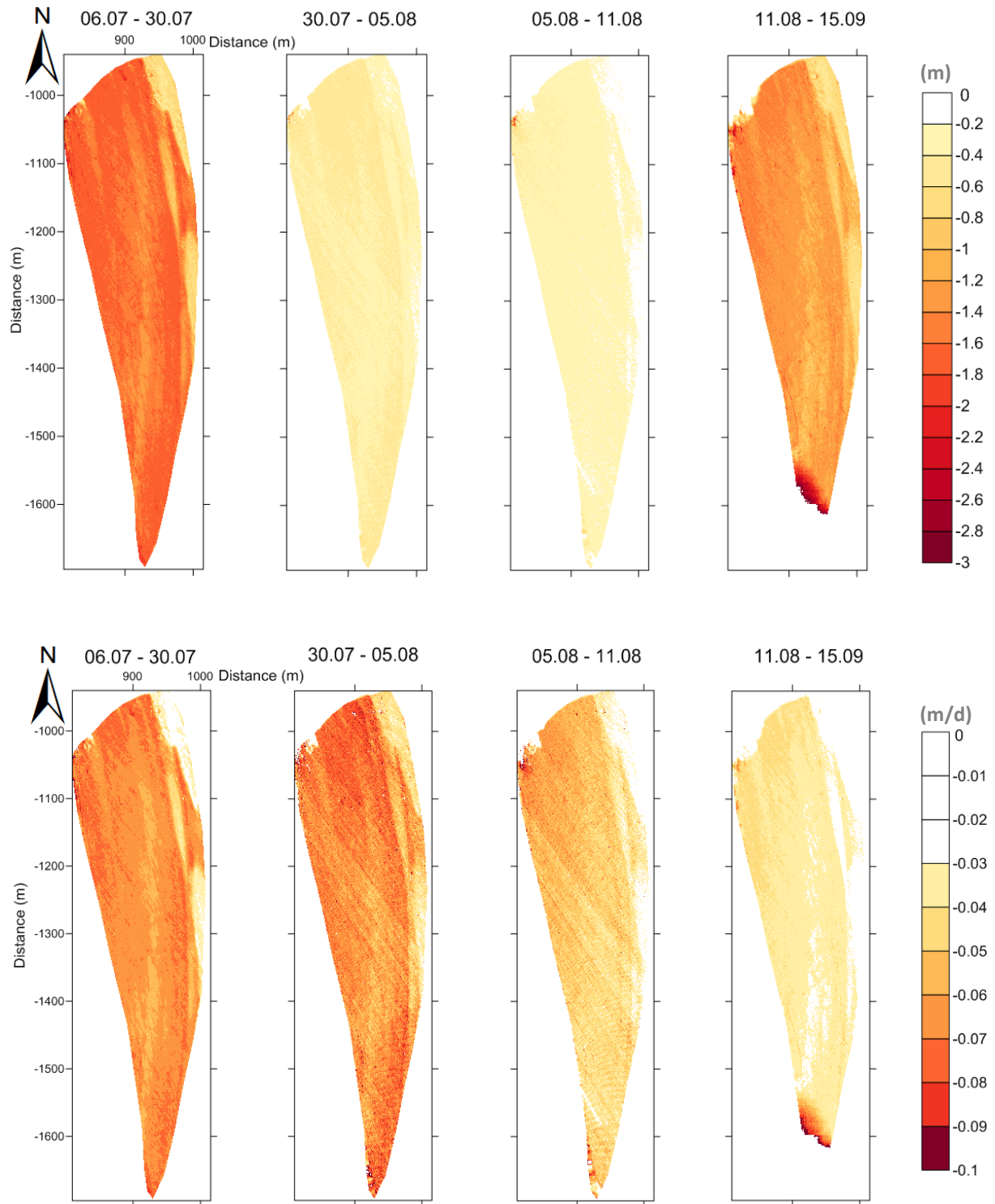


Figure 4: DEMs of difference for the seasonal survey

Above, the raw periodic melt rate (effective changes); below, the changes normalised by day

The axes are in the LiDAR co-ordinate system; the proportionality between the scale and the LoD was conserved



Figure 5: Outline of the seasonal survey shows on an old orthoimage (2009)

3.4.3 Surface changes at the intra-day scale

Figure 6 illustrates the DEMs of difference from 9h to 11h, 13h, 15h and 17h on the 5th August 2013. This day was one of the warmest days of the summer (Figure 3). There was no precipitation and a high insolation which increased the temperature rapidly (Figure 7). The maximal reached 22.9°C in Arolla at 13h. At this scale, it is possible to note two important elements of the surface change. The first is clear measurement of differential melt associated with ogives on the glacier surface. At the intra-day scale, given Mair *et al.* (2003), these cannot be related to down glacier movement of undulations in the ice surface, but rather must reflect differential melt rates associated with the effects of ogive-related differences in surface albedo. The second pattern is associated with a positive surface change in the up glacier portion of the study area, early in the morning, which decays progressively during the day.

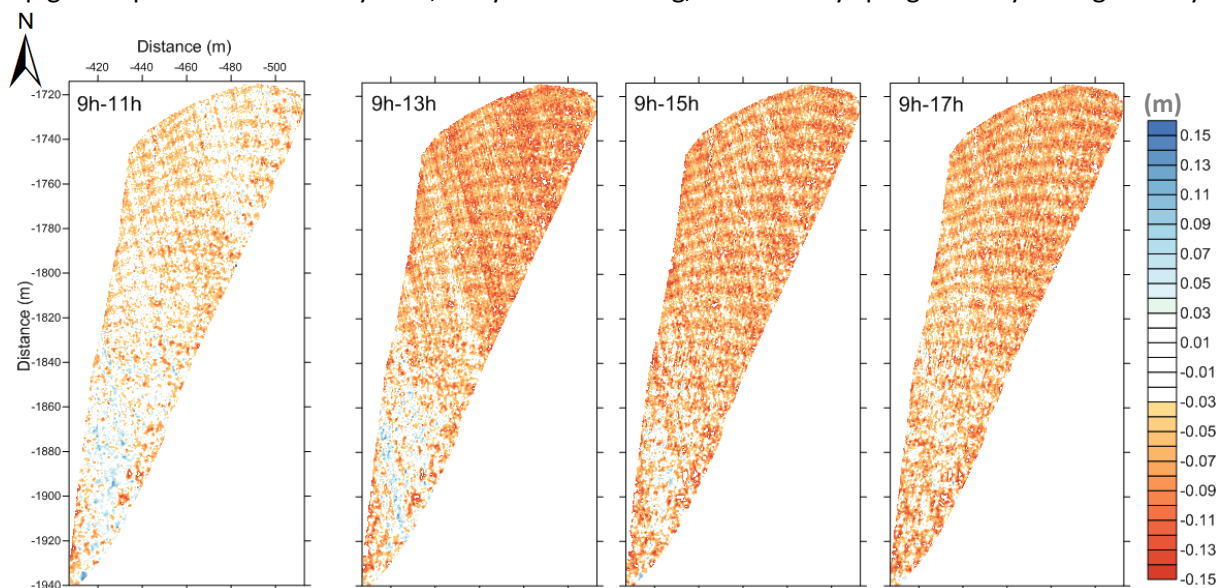


Figure 6: DEMs of difference for the intra-day survey
The axes are in the LiDAR co-ordinate system

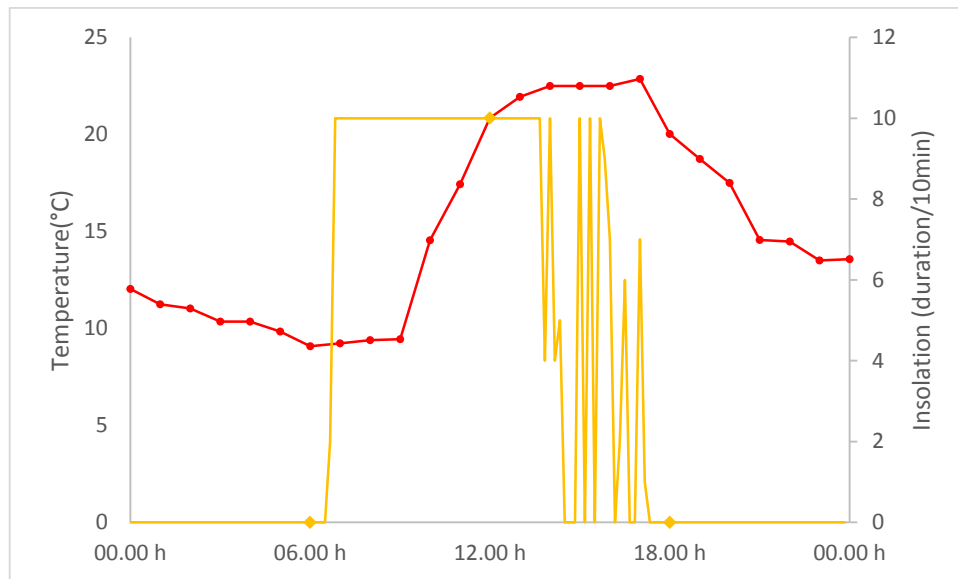


Figure 7: Temperatures and insolation conditions on the 05/08/2013

These values are issued from Evolène station (insolation - Météosuisse) and Arolla usine station (temperature - HYDRO Exploitation SA)

3.5 Discussion

3.5.1 Methodological issues and data quality

In methodological terms, this paper shows that long range terrestrial laser scanners that use wavelengths suitable for reflection by snow and ice are able to provide exceptional levels of detail on surface ice melt. Here, this was demonstrated with respect to both the seasonal and intra-day scales. These data were able to reveal spatial variability in melt related to moraine cover at the seasonal scale and the presence of ogives in the ice surface at the intra-day scale.

The typical survey distance for these measures was between 2 and 3 km and data with a mean spatial resolution of 0.17 m were obtained. The acquisition time for the larger seasonal scale area was less than c. 20 minutes and for the smaller intra-day scale area less than 8 minutes. Obtaining these data comes with the following caveats: (1) atmospheric absorption (clouds and rain) both reduce the possible survey distances and introduce substantial noise; (2) the actual scan areas had to be enlarged to allow measurement of zones (here bedrock outcrops) that could be guaranteed as fixed during the study periods; (3) better precision was possible where the scanner did not need to be moved between surveys (i.e. at the intra-day timescale); (4) use of the scanner required attention to be given to safety related issues; and (5) the complexity of the glacier surface may need more than a single scan position. In this case, only a single position was needed because a suitable vantage point of the glacier could be identified. These issues notwithstanding, the data obtained appeared to be highly realistic with only very minimal artefacts (e.g. Figure 4) present in the data. In theory, the scan can be used to provide highly reliable and spatially rich data on surface melt patterns, without further correction, provide that the time between scans is short as compared to the lateral glacier surface velocity. If the scanner is not moved between scans, and despite the 2 to 3 km distance from the area scanned, melt rates of 2 cm or greater could be measured.

3.5.2 Seasonal surface changes

There is a broad association between overall melt rates and the evolution of temperature and insolation from early June until mid-September.

The spatial variability in melt was clearly associated with the effects of debris cover related to medial moraines (Figure 5). The Haut Glacier d'Arolla possesses three medial moraines: an ablation-dominated moraine east of the glacier centre line, an ice-stream interaction moraine west of the glacier centre line, and a medial-lateral supraglacial moraine complex along the western margin of the glacier (Gomez *et al.*, 1985). The first corresponds to the linear-curved feature shape on the eastern part of the study area and the second is found in the centre of the figure (Figure 4). These melting differences result from debris cover thickness effects. A thin debris cover (<~5 cm) enhances ablation due to a reduced albedo and an increased absorption of shortwave radiation, whereas thicker debris insulates the underlying ice and reduces ablation, because of its low thermal conductivity (Nakawo *et al.*, 1981). As the scanner also provides data on the reflectance properties of the surface, it is possible that in addition to obtaining surface melt rate data, it may also be able to infer debris cover characteristics, something that is planned to explore in future projects.

It was also possible to identify some aspect effects. The aspect of the study area is shown in Figure 8. The region that was the most exposed to the sun (dark red) during the summer coincides with the zone downstream where there was more melt. Obviously others parameters have to be mentioned to explain these changes in the mass balance, both meteorological and physical, but they show that there is work to be done to exploring how these data may be used to drive spatially distributed melt models.

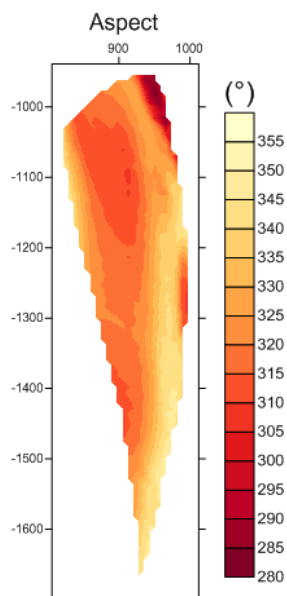


Figure 8: Aspect for the seasonal survey
The darker the red, the more the glacier received sun during the summer season 2013
Axis, distance in [m]

3.5.3 Intra-day surface changes

The ability to detect differential melt associated with ogives was surprising. Ogives are small scale debris bands that generally form annually (Benn *et al.*, 1998) and which can be considered as kinematic waves that are a consequence of inertial forces (Hooke, 2005). They characterise the overall ice flow direction (Benn *et al.*, 1998) and lead to patterns of cumulative strain that is greater at the glacier

margin with velocity greatest near the central-line (Hambrey *et al.*, 1980). Here, it was shown how they cause spatial patterns in surface melt.

The more intriguing part of these data is the measurement of surface uplift early on during the day that diminishes gradually to allow the ogive pattern to become dominant across the glacier. Such a change could have several origins: (1) a registration error, with one or more surfaces having an incorrect spatial trend; (2) the effects of differential ice flux which would lead to thickening in the upstream part of the area of interest; (3) the effects of aspect on differential surface melt; or (4) the effects of within day hydraulic jacking (e.g. Kulesa *et al.*, 2008). A check of the spatial distribution of the residuals to the fitted co-registration showed no spatial trend, so eliminating the first hypothesis. The second hypothesis can be evaluated by considering the magnitude of the observed changes. These are typically around 0.10 m in two hours (09h to 11h, Figure 6). That is, ice that is 0.10 m higher than any one grid cell will need to move downstream by 0.30 m, the grid cell resolution, in order for the magnitude of change to be due to an ice flux effect. In the area of uplift, the glacier surface slope is about 0.1. That is, there would need to be a lateral displacement of the glacier of about 1.0 m in 2 hours. This is almost an order of magnitude greater than the maximum daily velocities measured on the Haut Glacier d'Arolla, associated with relatively infrequent spring-melt related speed up events. It is highly unlikely. Additionally, feature tracking using the point clouds (e.g. of structural weaknesses evident in the surface) showed no lateral displacement at the 2 hours timescale.

The possibility that aspect and debris cover could explain this difference, even if correct, does not explain surface uplift. At the intra-day scale, it can be added that the slope down glacier was the same throughout the area. The aspect (Figure 9) showed that the upper part was probably subject to higher insolation, which also counters this explanation.

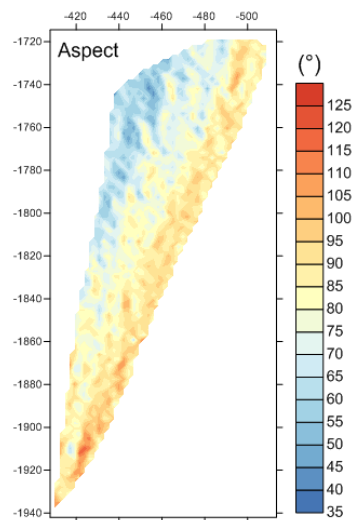


Figure 9: Aspect for the 05/08/2013
The darker the red, the more the glacier received sun on the 05/08/2013
Axis, distance in [m]

The hypothesis that remains is that some kind of intra-day hydraulic jacking was measured. Kulesa *et al.* (2008) suggest that this may happen at a sub-daily scale associated with the onset of melting and the associated local build up of subglacial water pressure. This phenomenon has not been observed at the Haut Glacier d'Arolla and, indeed, if it is a local effect, the density of the net of point measurements required to detect it is higher than those densities typically used at this glacier.

With other hypotheses excluded, it may be that the surface uplift could be thus describing a hydraulic jacking effect associated with subglacial hydrological processes. The transition from a distributed to a

canalised system has been observed and explained at seasonal scale (e.g. Nienow *et al.*, 1998; Mair *et al.*, 2002a; Kulesa *et al.*, 2008; Mair *et al.*, 2008). The hydraulic jacking may occur because after partial closure of the channels overnight, there was a rapid input of melt water linked to high insolation and rapid temperature rise (Figure 7), at a rate that is greater than the capacity of the channels to melt (Hock *et al.*, 1993), such that the pressure builds up (Mair *et al.*, 2003). Afterward it followed an ice-bed decoupling, resulting from an uplift of the ice and a strengthening of the subglacial lubrication (Mair *et al.*, 2003). The fact that this is restricted to the upper part of the studied area may reflect the steep gradient in ice thickness up glacier, which will drive closure rates. To further evaluate this assumption, repeat survey of this area, coupled with measurements of subglacial channels using radar, is required.

3.6 Conclusions

This study has shown that elements of the melting and dynamic processes of an Alpine temperate valley glacier can be measured using long range terrestrial laser scanning. This was demonstrated using data obtained at two temporal scales: seasonal and intra-day. At the seasonal scale, mean melt rates of $0.05 \pm 0.002 \text{ m}^3/\text{m}^2$ per day, uncorrected for flux effects, were measured between July and mid-September. The data show how this melt rate declined with the transition from mid-summer to early autumn, and how it was spatially variable in relation to glacier debris cover. At the intra-day scale, differential melt was measured associated with ogive-related variability in debris cover as well as a possible hydraulic jacking early on during the day associated with temporary build up of subglacial water pressure.

At the spatial scale of study (a scan distance of 2 km to 3 km), use of a laser wavelength optimal for snow and ice cover allowed data to be obtained with a mean point spacing of less than 0.20 m. The surface changes that could be detected depended on: (1) whether or not the scanner was moved between surveys, leading to better precision at the within-day scale when the scanner was fixed; and (2) the quality of the co-registration process.

3.7 Acknowledgements

This study would not have been possible without the support of the University of Lausanne (UNIL) and the Fondation Herbette. Special thanks to Mattia Brughelli for his help during the field campaign and to Mauro Fischer for earlier comments on this work.

Part IV - Conclusion



Chapter picture
The sandur of the Haut Glacier d’Arolla

With the snow covered glacier as background (06/07/2013)

4.1 Overall conclusion

4.1.1 Glacier recession and climate forcing

The Haut Glacier d'Arolla has been in continuous recession since 1967, associated with a progressive temperature rise. This is despite the snowier and colder periods recorded in Switzerland in the late 1970s and early 1980s during which most Swiss glaciers advanced (Haeberli *et al.*, 1998), including adjacent ones (Bas Glacier d'Arolla; Tsijiore Nouve). Although the snowier/colder period may have increased ice accumulation in the upper glaciated part of the basin, the low rate of ice flux was insufficient to prevent a continued thinning and snout recession. Thus, unlike other glaciers, the duration of the snowier/colder period was too short to translate into a glacier advance, that is it has too long a response time, and continual recession was recorded. The long response time is probably a function of the low glacier surface slope.

4.1.2 Glacier melt dynamics at three time scales

The combination of the decadal scale photogrammetric survey with the seasonal and intra-day laser scanning surveys allowed different rates of melt to be calculated. Melt rates were highest down glacier, reflecting snout retreat. In addition, because of the glacier configuration, spatial patterns of melt showed substantial variability, clearly related to the effects of debris cover on melt, and moraine formation. The Haut Glacier d'Arolla possesses three medial moraines: an ablation-dominated moraine east of the glacier centre line, an ice-stream interaction moraine west of the glacier centre line, and a medial-lateral supraglacial moraine complex along the western margin of the glacier (Gomez *et al.*, 1985). Both at the decadal and the seasonal scales, the melt rates were higher on the ice, and lowest on the moraines reflecting debris-cover insulation. By contrast, at the intra-day scale, enhanced melt rates were noted where there was debris related to ogives but where the cover was less thick, associated with increased albedo but where the debris cover was not sufficient to insulate the ice.

4.1.3 Glacier dynamics at three time scales

It was possible to study glacier dynamics at two of the three time scales. At the decadal scale, the flux was measured by tracking surface particles and combining this with data on bed geometry. This showed some variability in ice mass flux, but flux rates were generally always much smaller than the volumes of ice per year being lost in the glacier margin. This was the reason for the rapid glacier retreat.

At the intra-day scale, a pattern of surface uplift was observed early in the morning. Though the process of elimination of other hypotheses, this was concluded as most likely to be a hydraulic jacking effect associated with subglacial hydrological processes. Overnight reductions in subglacial channel capacity coupled to rapid rises in melt rates early in the morning combined to increase subglacial water pressure sufficiently, and leading to surface uplift. Further work is required to confirm this conclusion.

4.1.4 Methodological issues

This study demonstrated the relevance of using remote sensing technologies in glacier research. In particular, the potential of archival digital photogrammetry to reconstruct glacier advance and recession was proved. Provided that certain conditions are met, it was possible to generate data with a very good precision in the vertical and so to detect surface changes of better than ± 0.3 m over quite long time periods.

This study also showed that long range terrestrial laser scanners that use wavelengths suitable for reflection by snow and ice are able to provide exceptional levels of detail on surface ice melt. The typical survey distance for these measures was between 2 and 3 km and data with a mean spatial resolution of 0.17 m were obtained. When the scanner was not moved between scans, surface changes of 2 cm or greater could be measured. Moreover, the error analysis produced encouraging results in both approaches with a very low error rate all along the processes.

Thus, archival digital photogrammetry can provide valuable data on glacier response to climate forcing over multiple decades for unmonitored glaciers, where imagery is available, and data obtained by terrestrial laser scanning appeared to be highly realistic with only very minimal artefacts. These methods offer thereby highly reliable and spatially rich and precise data on surface change patterns at different time scales.

4.2 Limits and perspectives

Technically, a number of critical perspectives have to be noted. Photogrammetry used in order to reconstruct past events needs historical imagery, which has to be available with a good enough temporal resolution and a spatial scale that allows detection of detail while having sufficient overlapping ground coverage. To ensure the products quality, the glacier surface has to be no snow covered, no cloud covered and not shadowed by the mountains around during image acquisition. Imagery acquired at the end of the summer ablation season is most likely to be optimal, but it is probably the case that in snowier years, there will be parts of the basin where it is not possible to estimate surface change for an entire glacier.

As regards LiDAR measurements, the terrain has to be readily accessible (given the bulky and fragile nature of the equipment), without moisture, without dust because of wind and without fog in the zone of interest. However, night acquisitions are possible. The use of the scanner requires attention to be given to safety related issues. There remained some artefacts in the results, including diagonal lines, related to small imprecisions in the orientation of individual laser lines. This inconvenience could be solved by combining scans from other points of view.

To augment the accuracy of the meteorological data (temperature, precipitation and insolation), it is important to use a closer meteorological station. Private data being collected by HYDRO Exploitation SA are now available and will be used in future work.

The zone has to be enlarged for the LiDAR data also, in order to confirm if the uplift phenomenon observed was really a hydraulic jacking and to better determine the spatial distribution of the changes

in depth. In the same way, the surface surveys could be associated with below surface data acquisitions (Ground Penetration Radar, seismic, borehole, etc.) to connect the processes. Moreover, a better precision is possible where the scanner does not need to be moved between surveys or if a GPS is connected to the device. This improvement would reduce the stereo-matching error margin and would directly give a co-ordinate system, which has to be considered in the forthcoming investigations.

The very high quality products created during this research allowed determination of glacier changes and dynamics over time by computing calculations on DEMs and DEMs of difference. To continue with this work, evolution of the erosion and deposition areas around the glacier at the decadal scale could be analysed and a focus could be established on the sandur for instance. Another focus could be the impacts of glacier retreat for future hydroelectric development exploitation. Overall, the potentially most intriguing and interesting measurement to follow up is probably the surface uplift early on during the day that diminishes gradually.

4.3 References

- Abermann, J., Lambrecht, A., Fischer, A., and Kuhn, M. (2009). Quantifying changes and trends in glacier area and volume in the Austrian Ötztal Alps (1969-1997-2006). *The Cryosphere*, 3, 205–215.
- Alean, J. and Hambrey, M. (2008). *Glaciers online – Glaciers of the Alps – Haut Glacier d’Arolla* [Web Page]. Available on: http://www.swisseduc.ch/glaciers/alps/haut_glacier_d_arolla/ (Viewed on the 03.04.2012).
- Alho, P., Kukko, A., Hyyppä, H., Kaartinen, H., Hyyppä, J. and Jaakkola, A. (2009). Application of boat-based laser scanning for river survey. *Earth Surface Processes and Landforms*, 34, 1831-1838.
- Andreassen, L. M., Elvehoy, H. and Kjollmoen, B. (2002). Using aerial photography to study glacier changes in Norway. *Annals of Glaciology*, 34, 343–348.
- Arnold, N. (2005). Investigation the sensitivity of glacier mass-balance/elevation profiles to changing meteorological conditions: Model experiments for Haut Glacier d’Arolla, Valais, Switzerland. *Arctic, Antarctic and Alpine Research*, 37(2), 139-145.
- Avian, M. and Bauer, A. (2006). First results on monitoring glacier dynamics with the aid of Terrestrial Laser Scanning on Pasterze Glacier (Hohe Tauern, Austria). *Grazer Schriften der Geographie und Raumforschung*, 41, 27-36.
- Baltsavias, E., Fayer, E., Bauder, A., Bösch, H. and Pateraki, M. (2001). Digital surface modelling by airborne laser scanning and digital photogrammetry for glacier monitoring. *Photogrammetric Record*, 17(98), 243-273.
- Barrand, N., Murray, T., James, T., Barr, S. and Mills, J. (2009). Optimizing photogrammetric DEMs for glacier volume change assessment using laser-scanning derived ground-control points. *Journal of Glaciology*, 55(189), 106-116.
- Bauer, A., Paar, G. and Kaufmann, V. (2003). Terrestrial laser scanning for rock glacier monitoring. In Phillips, M., Springman, S. M. and Arenson, L. U. (Eds), *Permafrost*, 55-60. UK: Taylor and Francis.
- Benn, D. I. and Evans, D. J. A. (1998). *Glaciers and Glaciations*. London: Arnold publisher.
- Benn, D. I., Kirkbride, M. P., Owen, L. A. and Brazier, V. (2003). Glaciated valley landsystems. In Evans, D.J.A. (Ed.), *Glacial Landsystems*, 372–406. London: Arnold.
- Brecher, H. H. (1986). Surface velocity determination on large polar glaciers by aerial photogrammetry. *Annals of Glaciology*, 8, 22-26.
- Brock, B. W. and Arnold, N. S. (2000a). A spreadsheet-based (Microsoft Excel) point surface energy balance model for glacier and snow melt studies. *Earth Surface Processes and Landforms*, 25(6), 649-658.
- Brock, B. W., Willis, I. C. and Sharp, M. J. (2000b). Measurement and parameterization of albedo variations at Haut Glacier d’Arolla, Switzerland. *Journal of Glaciology*, 46(155), 675-688.
- Brock, B. W., Willis, I. C. and Sharp, M. J. (2006). Measurement and parameterization of aerodynamic roughness length variations at Haut Glacier d’Arolla, Switzerland. *Journal of Glaciology*, 52(177), 281-297.
- Brock, B., Willis, I., Sharp, M. and Arnold, N. (2000c). Modelling seasonal and spatial variations in the surface energy balance of Haut Glacier d’Arolla, Switzerland. *Annals of Glaciology*, 31, 53-62.
- Chandler, J. (1999). Technical communication – Effective application of automated digital photogrammetry for geomorphological research. *Earth Surface Processes and Landforms*, 24, 51-63.
- Cogley, J. G., Hock, R., Rasmussen, L. A., Arendt, A. A., Bauder, A., Braithwaite, R. J., Jansson, P., Kaser, G., Möller, M., Nicholson L. and Zemp, M. (2011). *Glossary of glacier mass balance and related*

- terms, *IHP-VII Technical documents in hydrology No. 86, IACS, contribution No. 2*. Paris: UNESCO-International Hydrological Programme.
- Cooper, M. A. R. (1998). Datums, coordinates and differences. In Lane, S. N., Richards K. S. and Chandler J. H. (Eds), *Landform Monitoring, Modelling and Analysis*, 21-36. Chichester: John Wiley and Sons Ltd.
- Cracknell, A. and Hayes, L. (1991). *Introduction to Remote Sensing*. London: Taylor and Francis Editions.
- Dadic, R., Mott, R., Lehning, M. and Burlando, P. (2010). Wind influence on snow depth distribution and accumulation over glaciers. *Journal of Geophysical Research*, 115(F01012), 1-8.
- Deems, J., Painter, T. and Finnegan, D. (2013). LiDAR measurement of snow depth: a review. *Journal of Glaciology*, 59(215), 467-479.
- Diolaiuti, G. A., Bocchiola, D., Vagliasindi, M., D'Agata, C., and Smiraglia, C. (2012). The 1975-2005 glacier changes in Aosta Valley (Italy) and the relations with climate evolution. *Progress in Physical Geography*, 36(6), 764–785.
- ERDAS (2009). *LPS Project Manager – User's Guide*. USA: Author.
- Fagan, B. (2000). *The Little Ice Age – How climate made History, 1300-1850*. New York: Basic Books.
- Finsterwalder, S. (1890). Die Photogrammetrie in den italienischen Hochalpen. *Mittheilungen des Deutschen und Österreichischen Alpenvereins*, 16(1), 6-9.
- Fischer, M., Huss, M., Barboux, C. and Hoelzle, M. (In press). The new Swiss Glacier Inventory SGI2010: Relevance of using high-resolution source data on areas dominated by very small glaciers. *Arctic, Antarctic, and Alpine Research*.
- Fischer, U., Mair, D., Kavanaugh, J., Willis, I., Nienow, P. and Hubbard, B. (2011). Modelling ice-bed coupling during a glacier speed-up event: Haut Glacier d'Arolla, Switzerland. *Hydrological Processes*, 25, 1361-1372.
- Forel, F.-A. and Du Pasquier, L. (1986). Les variations périodiques des glaciers. 1er rapport, 1895. *Archives des Sciences physiques et naturelles, Genève*, 1012,(4,2), 129-147.
- Franco, B. and Vincent, C. (2010). *Les glaciers à l'épreuve du climat*. Marseille : Institut de recherche pour le développement, IRD Éditions.
- Gabbud, C. and Lane, S. N. (submitted). Response of an Alpine valley glacier to climate change at decadal scale: The case of the Haut Glacier d'Arolla.
- Golden Software (2012). *Surfer® – Quick Start Guide – Contouring and 3D Surface Mapping for Scientists and Engineers*. Colorado: Author. Available on: <http://www.goldensoftware.com> (Viewed on the 19.12.2013).
- Gomez, B. and Small, R. J. (1985). Medial moraines of the Haut Glacier d'Arolla, Valais, Switzerland: Debris supply and implications for moraine formation. *Journal of Glaciology*, 31(109), 303-307.
- Haeberli, W. (1990). Glacier and permafrost signals of 20th-century warming. *Annals of Glaciology*, 14, 99-101.
- Haeberli, W. and Beniston, M. (1998). Climate change and its impacts on glaciers and permafrost in the Alps. *Ambio*, 27, 258 – 265.
- Haeberli, W., Müller, P., Alean, P. and Bösch, H. (1989). Glacier changes following the Little Ice Age – A survey of the international data basis and its perspectives. In J. Oerlemans (Ed.), *Glacier fluctuations and Climatic Change*, 77-101.
- Hambrey, M. J., Milnes, A. G. and Siegenthaler, H. (1980). Dynamics and structure of Griesgletscher, Switzerland. *Journal of Glaciology*, 25, 215-228.
- Harbor, J., Sharp, M., Copland, L., Hubbard, B., Nienow, P. and Mair, D. (1997). Influence of subglacial drainage conditions on the velocity distribution within a glacier cross section. *Geology*, 25, 739-742.

- Heid, T. and Käab, A. (2012). Repeat optical satellite images reveal widespread and long term decrease in land-terminating glacier speeds. *The Cryosphere*, 6, 467-478.
- Helfricht, K., Kuhn, M., Keuschning, M. and Heilig, A. (2013). LiDAR snow cover studies on glacier surface: significance of snow- and ice dynamical processes. *The Cryosphere Discussion*, 7, 1787-1832.
- Heritage, G., and Hetherington, D. (2007). Towards a protocol for laser scanning in fluvial geomorphology. *Earth Surface Processes and Landforms*, 32, 66-74.
- Herman, F., Anderson, B. and LePrince, S. (2011). Mountain glacier velocity variation during a retreat/advance cycle quantified using sub-pixel analysis of ASTER images. *Journal of Glaciology*, 57(202), 197-207.
- Hock, R. and Hooke, R. LeB. (1993). Evolution of the internal drainage system in the lower part of the ablation area of Storglaciären, Sweden. *Bulletin of the Geological Society of America*, 105(4), 537-546.
- Hodge, R., Brasington, J., and Richards, K. (2009). In situ characterization of grain-scale fluvial morphology using Terrestrial Laser Scanning. *Earth Surface Processes and Landforms*, 34, 954-968.
- Hooke, R. LeB. (2005). *Principles of glacier mechanics – Second Edition*. Cambridge: Cambridge University Press.
- Houghton, J. T., Meiria Filho, L. G., Callander, B. A., Harris, N., Kattenberg, A. and Maskell, K. (1996). *Climate Change 1995: the Science of Climate Change. Published for the Intergovernmental Panel on Climate Change*. Cambridge: University Press.
- Hubbard, A., Blatter, H., Nienow, P., Mair, D. and Hubbard, B. (1998). Comparison of a three-dimensional model for glacier flow with field data from Haut Glacier d'Arolla, Switzerland. *Journal of Glaciology*, 44(147), 368-278.
- Hubbard, A., Willis, I., Sharp, M., Mair, D., Nienow, P., Hubbard, B. and Blatter, H. (2000). Glacier mass-balance determination by remote sensing and high-resolution modelling. *Journal of Glaciology*, 46(154), 491-498.
- Hubbard, B. and Nienow, P. (1997). Alpine subglacial hydrology. *Quaternary Science Reviews*, 16, 939-955.
- Huss, M., Usselman, S., Farinotti, D. and Bauder, A. (2010). Glacier mass balance in the south-eastern Swiss Alps since 1900 and perspectives for the future. *Erkunde*, 64(2), 119-140.
- Iken, A. I., Röthlisberger, H., Flotron, A. and Haerberli, W. (1983). The Uplift of Unteraargletscher at the beginning of the melt season – A consequence of water storage at the bed? *Journal of Glaciology*, 29(191), 28-47.
- IPCC Intergovernmental Panel on Climate Change (2008). Technical Paper VI – French. Chapitre 3 – Relation entre le changement climatique et les ressources en eau : incidences et mesures d'intervention. In Bates, B. C, Kundzewicz, Z. W., Wu, S. and Palutikof, J. P., (Eds). *Climate Change and Water* (pp. 39-62). Geneva: IPCC Secretariat.
- IPCC Intergovernmental Panel on Climate Change (2013). *Climate Change 2013 – The Physical Science Basis. Working Group I Contribution to the Fifth Assessment Report of the Intergovernmental Panel on Climate Change – WMA/UNEP*. UK: Cambridge University Press.
- Johannesson, T., Raymond, O., Laumann, T. and Kennett, M. (1989). Timescale for adjustment of glaciers to changes in mass balance. *Journal of Glaciology*, 35, 355-369.
- Käab, A. (2001). Photogrammetric reconstruction of glacier mass-balance using a kinematic ice-flux model. A 20-year time-series on Grubengletscher, Swiss Alps. *Annals of Glaciology*, 31, 45-52.
- Kasser, P. (1967). *Fluctuations of glaciers 1959-1965*. Paris: IAHS and UNESCO.

- Keutterling, A. and Thomas, A. (2006). Monitoring glacier elevation and volume changes with digital photogrammetry and GIS at Gepatschferner glacier, Austria. *International Journal of Remote Sensing*, 27(19), 4371-4380.
- Kulesa, B., Hubbard, B., Brown, G. and Becker, J. (2003). Earth tide forcing of glacier drainage. *Geophysical Research Letters*, 30(1), 11-1 - 11-4.
- Lane, S. (2012). *Arolla, climatologie mensuelle, 1864-2012 (with open access Meteosuisse data)* [Excel data table]. Available on: http://ebibalpin.unil.ch/document/donnees_climat (Viewed on the 06.04.2014).
- Lane, S. N., Westaway, R. M. and Hicks, D. M. (2003). Estimation of erosion and deposition volumes in a large, gravel-bed, braided river using synoptic remote sensing. *Earth Surface Processes and Landforms*, 28, 249-271.
- Lane, S. N., Widdison, P. E., Thomas, R. E., Ashworth, P. J., Best, J. L., Lunt, I. A., Smith, G. H. S. and Simpson, C. J. (2010). Quantification of braided river channel change using archival digital image analysis. *Earth Surface Processes and Landforms*, 35(8), 971-985.
- Mair, D., Hubbard, B., Nienow, P., Willis, I., Fischer, U. H. (2008). Diurnal fluctuations on glacier ice deformation: Haut Glacier d'Arolla, Switzerland. *Earth Surface Processes and Landforms*, 33, 1272-1284.
- Mair, D., Nienow, P., Sharp, M., Wohlleben, T. and Willis, I. (2002a). Influence of subglacial drainage system evolution on glacier surface motion: Haut Glacier d'Arolla, Switzerland. *Journal of Geophysical Research*, 107(0), X-1 - X-13.
- Mair, D., Sharp, M. and Willis, I. (2002b). Evidence for basal cavity opening from analysis of surface uplift during a high-velocity event: Haut Glacier d'Arolla, Switzerland. *Journal of Glaciology*, 48(161), 208-216.
- Mair, D., Willis, I., Fischer, U., Hubbard, B., Nienow, P. and Hubbard, A. (2003). Hydrological controls on patterns of surface, internal and basal motion during three "spring events": Haut Glacier d'Arolla, Switzerland. *Journal of Glaciology*, 49(167), 555-567.
- Maisch, M. (2000). The longterm signal of climate change in the Swiss Alps: Glacier retreat since the end of the Little Ice Age and future ice decay scenarios. *Geografia Fisica e Dinamica Quaternaria*, 23, 139-151.
- Matthews, J. A. and Briffa, K. R. (2005). The 'Little Ice Age': Re-evaluation of an evolving concept. *Geografiska Annaler*, 87(1), 17-36.
- Mercanton, P.-L. (1961). Rapport sur les variations de longueur des glaciers européens en 1956-57; 1957-58 et 1958-59. *IAHS Publication*, 54, 366-378.
- MétéoSuisse (2010). *Bulletin climatologique annuel – rétrospective annuelle 2009* [Web Page]. Available on : http://www.meteosuisse.admin.ch/web/fr/climat/climat_aujourd'hui/retrospective_annuelle/flash2009.html (Viewed on the 01.07.2014).
- Nakawo, M., and Young, G. J. (1981). Field experiments to determine the effect of a debris layer on ablation of glacier ice. *Annals of Glaciology*, 2, 85-91.
- Nienow, P., Sharp, M. and Willis, I. (1998). Seasonal changes in the morphology of the subglacial drainage system, Haut Glacier d'Arolla, Switzerland. *Earth Surface Processes and Landforms*, 23, 825-843.
- Nienow, P. W., Hubbard, A. L., Hubbard, B. L., Chandler, D. M., Mair, D. W. F., Sharp, M. J. and Willis, I. C. (2005). Hydrological controls on diurnal ice flow variability in valley glaciers. *Journal of Geophysical Research*, 110(F04002), 1-11.

- Notebaert, B., Verstraeten, G., Govers, G. and Poesen, J. (2009). Qualitative and quantitative applications of LiDAR imagery in fluvial geomorphology. *Earth Surface Processes and Landforms*, 34, 217-231.
- OcCC Organe consultatif sur les Changements Climatiques et ProClim- (2007). *Les changements climatiques et la Suisse en 2050 ; Impacts attendus sur l'environnement, la société et l'économie*. Berne : auteurs.
- OFEV Office Fédéral de l'Environnement et MétéoSuisse Office Fédéral de Météorologie et de Climatologie (2013). *Changements climatiques en Suisse – Indicateurs des causes, des effets et des mesures*. Berne: auteurs.
- ONERC Observation National sur les Effets du Réchauffement Climatique (2008). *Changements climatiques dans les Alpes : Impacts et risques naturels. Rapport technique N°1*. Paris : auteur.
- Paterson, W. S. B. (1994). *The physics of glaciers – Third Edition*. Kidlington: Elsevier Science Ltd.
- Pellicciotti, F., Brock, B., Strasser, U., Burlando, P., Funk, M. and Corripio, J. (2005). An enhanced temperature-index glacier melt model including the shortwave radiation balance: development and testing for Haut Glacier d'Arolla, Switzerland. *Journal of Glaciology*, 57(175), 573-587.
- Pellikka, P. and Rees, W. G. (2010). *Remote Sensing of glaciers – Techniques for topographic, spatial and thematic mapping of glaciers*. London: Taylor and Francis Group.
- Rees, W. and Arnold, N. (2007). Mass balance and dynamics of a valley glacier measured by high-resolution LiDAR. *Polar Record*, 43(227), 311-319.
- Reinhardt, W. and Rentsch, H. (1986). Determination of changes in volume and elevation of glaciers using digital elevation models from the Vernagtferner, Ötztal Alps, Austria. *Annals of Glaciology*, 8, 151-155.
- RIEGL, Laser Measurement Systems (2005). *RiSCAN PRO® – Version 1.2.0sp1*. Austria: Author.
- RIEGL, Laser Measurement Systems (2012). *Instruction Manual - RIEGL VZ-6000 Safety Guidelines*. Austria: Author.
- RIEGL, Laser Measurement Systems (2013a). *New- RIEGL VZ-6000* [Web Page]. Available on: <http://www.riegl.com/nc/products/terrestrialscanning/produktdetail/product/scanner/33/> (Viewed on the 17.04.2013).
- RIEGL, Laser Measurement Systems (2013b). *Preliminary Data Sheet, 07.05.2013; RIEGL VZ-6000 – 3D Ultra long range terrestrial laser scanner with online waveform processing*. Austria: Author.
- RIEGL, Laser Measurement Systems (2013c). *3D Terrestrial Laser Scanner – RIEGL VZ-4000 / RIEGL VZ-6000; General Description and Data Interfaces*. Austria: Author.
- Rippin, D. M., Willis, I., Arnold, N. S., Hodson, A., Moore, J., Kohler, J. and Björnsson, H. (2003). Changes in geometry and subglacial drainage of Midre Lov'enbreen, Svalbard, determined from digital elevation models. *Earth Surface Processes and Landforms*, 28, 273-298.
- Scherler, D., Leprince, S. and Strecker, M. R. (2008). Glacier-surface velocities in alpine terrain from optical satellite imagery-Accuracy improvement and quality assessment. *Remote Sensing of Environment*, 112, 3806-3819.
- Schwalbe, E., Maas, H.-G., Dietrich, R. and Ewert, H. (2008). Glacier velocity determination from multi temporal terrestrial long range laser scanner point clouds. *XXIst ISPRS Congress: Commission V, WG3, Beijing*, 457-462.
- Seroussi, H., Morlighem, M., Rignot, E., Larour, E., Audry, D., Ben Dhia, H. and Kristensen, S. S. (2011). Ice flux divergence anomalies in 79north Glacier, Greenland. *Geophysical Research Letters*, 38(L09501), 1-5.

- Sharp, M. J., Richards, K. S., Willis, I. C., Arnold, N. S. and Nienow, P. (1993). Geometry, bed topography and drainage system structure of the Haut Glacier d'Arolla, Switzerland. *Earth Surface Processes and Landforms*, 18, 557-571.
- Small, R. J., Beecroft, I. R. and Stirling, D. M. (1984). Rate of deposition on lateral moraine embankments, Glacier de Tsidjore Nouve, Valais, Switzerland. *Journal of Glaciology*, 30(106), 275-181.
- Smith, M., Varicat, D. and Gibbins, C. (2012). Through-water terrestrial laser scanning of gravel beds at the patch scale. *Earth Surface Processes and Landforms*, 37, 411-21.
- Swift, D. A., Nienow, P. W., Spedding, N. and Hoey, T. B. (2002). Geomorphic implications of subglacial drainage system configuration: rates of basal sediment evacuation controlled by seasonal drainage system evolution. *Sedimentary Geology*, 149, 5-19.
- WAV Laboratory of Hydraulics, Hydrology and Glaciology (2013). *Glaciological reports (1881-2009). The Swiss Glaciers – Yearbooks of the Cryospheric Commission of the Swiss Academy of Sciences (SCNAT) published since 1964*. Zürich: ETH. Available on: <http://glaciology.ethz.ch/swiss-glaciers/> (Viewed on the 22.07.2014).
- Williams, R. D., Brasington, J., Vericat, D. and Hicks, D. M. (2013). Hyperscale terrain modelling of braided rivers: fusing mobile terrestrial laser scanning and optical bathymetric mapping. *Earth Surface Processes and Landforms*, 39(2), 167-183.
- Willis, I., Mair, D., Hubbard, B., Nienow, P., Fischer, U. and Hubbard, A. (2003). Seasonal variations in ice deformation and basal motion across the tongue of Haut Glacier d'Arolla, Switzerland. *Annals of Glaciology*, 36, 157-167.
- WMO World Meteorological Organization (1983). Report of the meeting on climate system monitoring, Geneva, 5-9 December 1983. *WMO/WCP-64*.
- Zhang, Z. (1992). Iterative point matching for registration of free-form curves. *International Journal of Computer Vision*, 13, 119-152.
- Zryd, A. (2001). *La nature dans les Alpes – Les Glaciers*. Saint-Maurice : Éditions Pillet.

